Measurements of integrated and differential cross sections for isolated photon pair production in 8 TeV pp collisions at ATLAS.

Rencontres de Moriond: QCD and High Energy Interactions

Matthias Saimpert, on behalf of ATLAS

Deutsches Elektronen-Synchrotron (DESY)

March 30th, 2017

HELMHOLTZ GEMEINSCHAFT

DESY

Photon pair production at the LHC

- The $\gamma\gamma$ final-state at the LHC is mostly known as a Higgs discovery channel and for having produced a legendary number of theory papers in 2015-2016.

Photon pair production at the LHC

- The $\gamma\gamma$ final-state at the LHC is mostly known as a Higgs discovery channel and for having produced a legendary number of theory papers in 2015-2016.
- But actually, most of the photon pairs at the LHC are produced in (rather) simple QCD interactions:

photon pair QCD production ($> 99\%$)

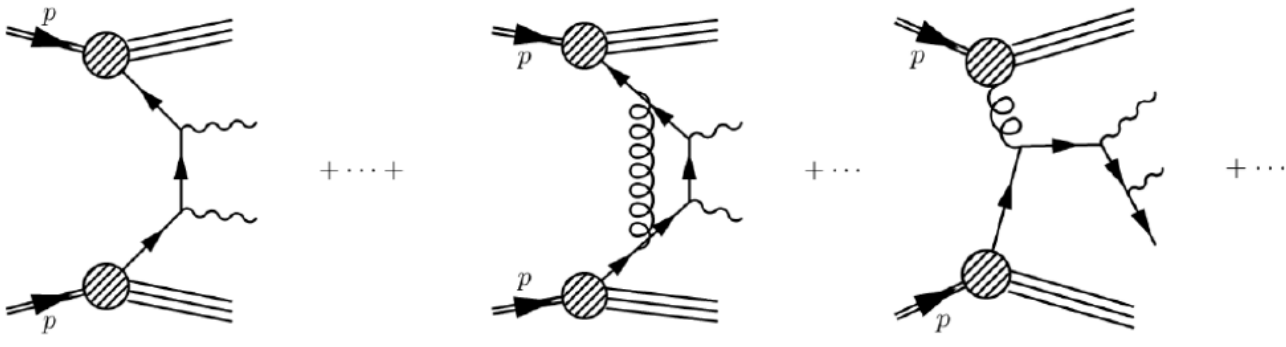

H $\rightarrow \gamma\gamma$ ($< 1\%$) and new phenomena (?)

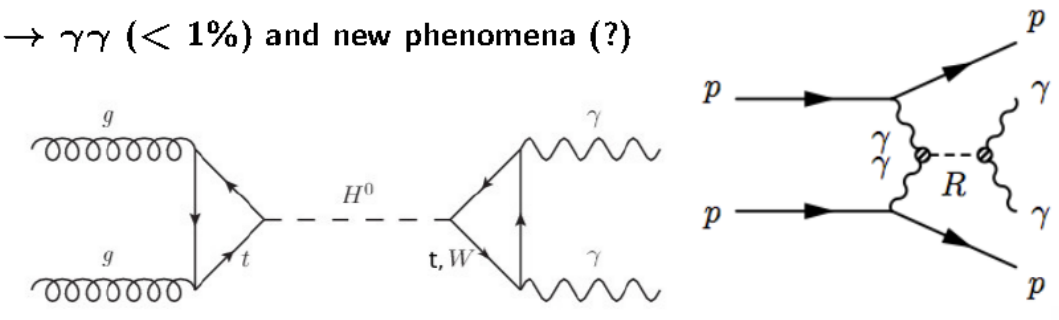

Photon pair production at the LHC

- The $\gamma\gamma$ final-state at the LHC is mostly known as a Higgs discovery channel and for having produced a legendary number of theory papers in 2015-2016.
- But actually, most of the photon pairs at the LHC are produced in (rather) simple QCD interactions:

photon pair QCD production ($> 99\%$)

- sensitive to α_s corrections

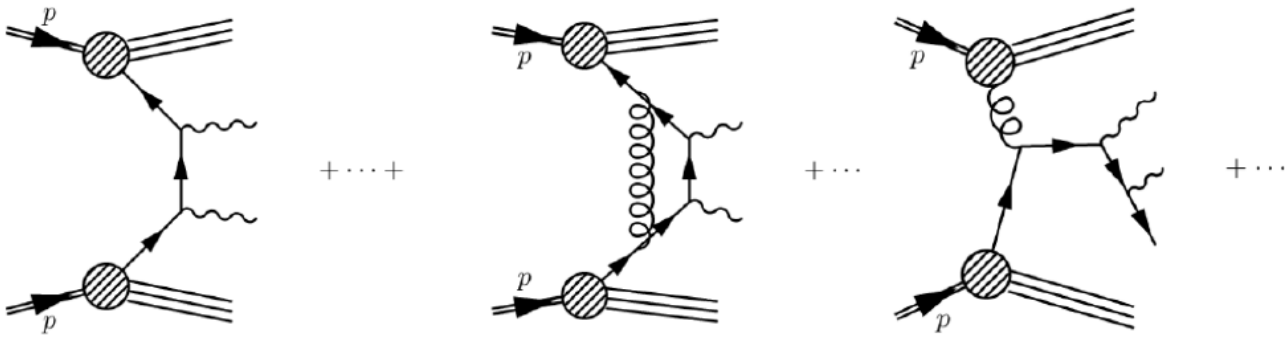

H $\rightarrow \gamma\gamma$ ($< 1\%$) and new phenomena (?)

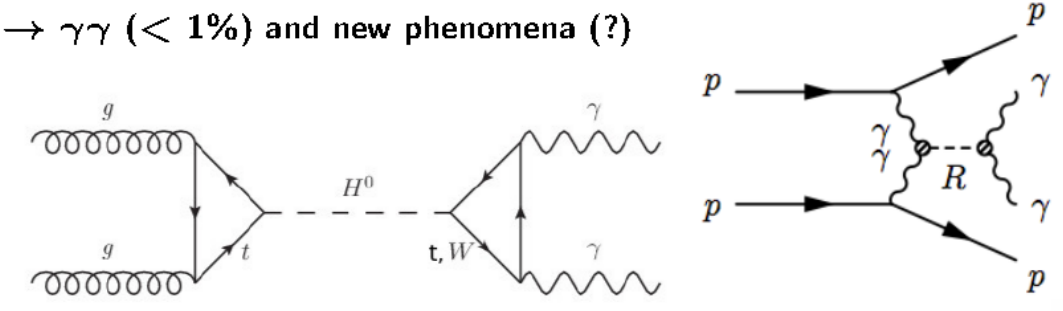

Photon pair production at the LHC

- The $\gamma\gamma$ final-state at the LHC is mostly known as a Higgs discovery channel and for having produced a legendary number of theory papers in 2015-2016.
- But actually, most of the photon pairs at the LHC are produced in (rather) simple QCD interactions:

photon pair QCD production ($> 99\%$)

- sensitive to α_s corrections
- sensitive to QCD infrared (IR) emissions ($m_{\gamma\gamma} >> p_{\mathrm{T},\gamma\gamma}$)

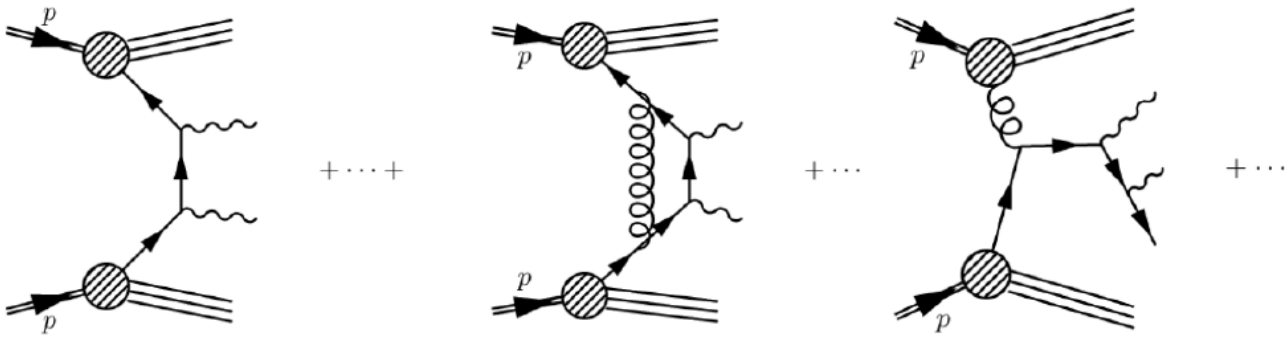

H $\rightarrow \gamma\gamma$ ($< 1\%$) and new phenomena (?)

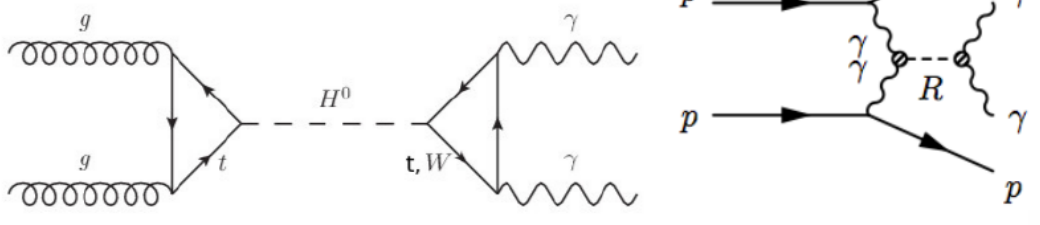

Photon pair production at the LHC

- The $\gamma\gamma$ final-state at the LHC is mostly known as a Higgs discovery channel and for having produced a legendary number of theory papers in 2015-2016.
- But actually, most of the photon pairs at the LHC are produced in (rather) simple QCD interactions:

photon pair QCD production ($> 99\%$)

- sensitive to α_s corrections
- sensitive to QCD infrared (IR) emissions ($m_{\gamma\gamma} >> p_{\mathrm{T},\gamma\gamma}$)
- main background for $H \to \gamma\gamma$

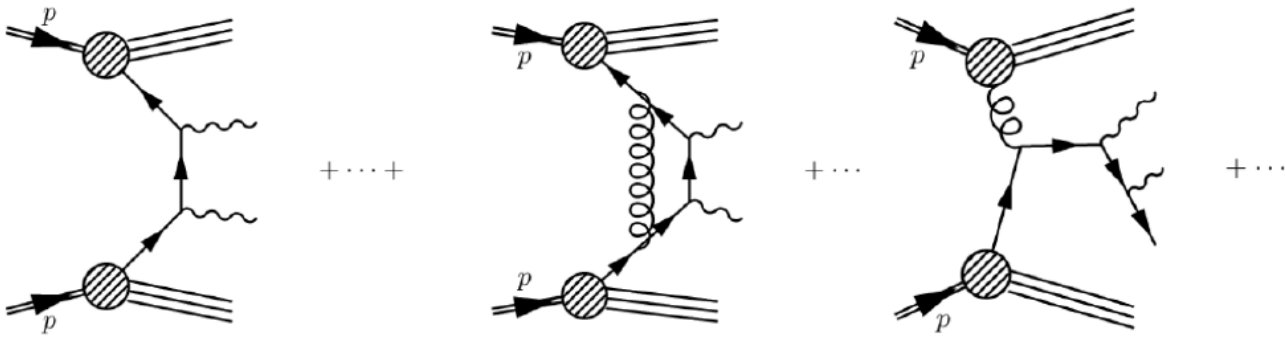

H $\to \gamma\gamma$ ($< 1\%$) and new phenomena (?)

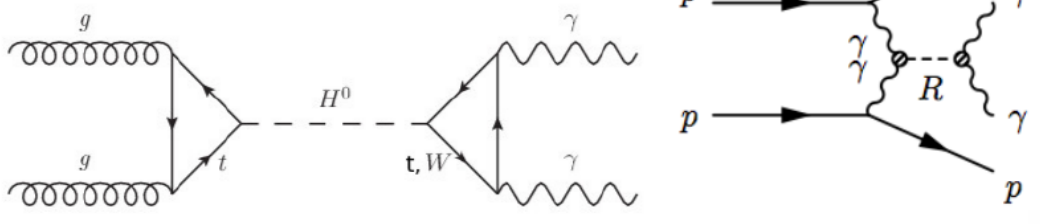

Photon pair production at the LHC

- The $\gamma\gamma$ final-state at the LHC is mostly known as a Higgs discovery channel and for having produced a legendary number of theory papers in 2015-2016.
- But actually, most of the photon pairs at the LHC are produced in (rather) simple QCD interactions:

photon pair QCD production ($> 99\%$)

- sensitive to α_s corrections
- sensitive to QCD infrared (IR) emissions ($m_{\gamma\gamma} >> p_{\mathrm{T},\gamma\gamma}$)
- main background for $H \to \gamma\gamma$
- possible window into new phenomena

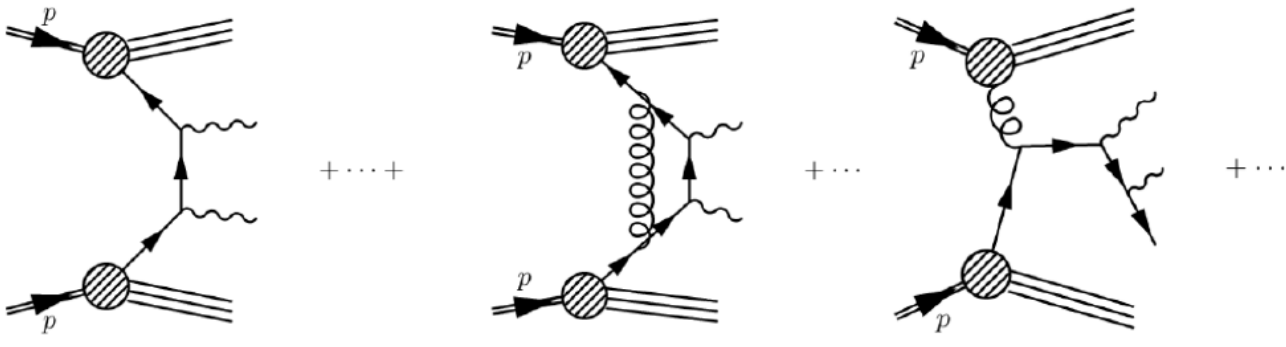

H $\to \gamma\gamma$ ($< 1\%$) and new phenomena (?)

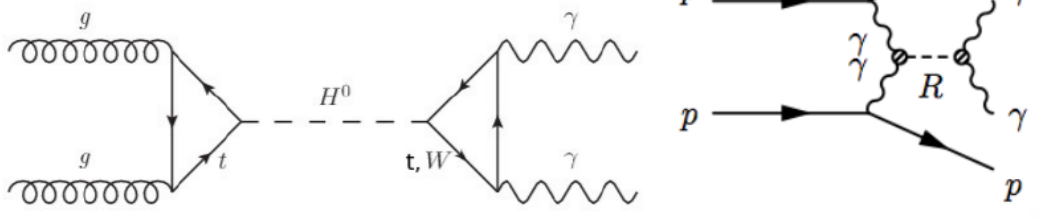

Photon pair production at the LHC

- The $\gamma\gamma$ final-state at the LHC is mostly known as a Higgs discovery channel and for having produced a legendary number of theory papers in 2015-2016.
- But actually, most of the photon pairs at the LHC are produced in (rather) simple QCD interactions:

photon pair QCD production ($> 99\%$)

- sensitive to α_s corrections
- sensitive to QCD infrared (IR) emissions ($m_{\gamma\gamma} >> p_{\mathrm{T},\gamma\gamma}$)
- main background for $H \to \gamma\gamma$
- possible window into new phenomena
- **New ATLAS measurement, $\sqrt{s} = 8$ TeV, 20.2 fb^{-1}, STDM-2015-15**

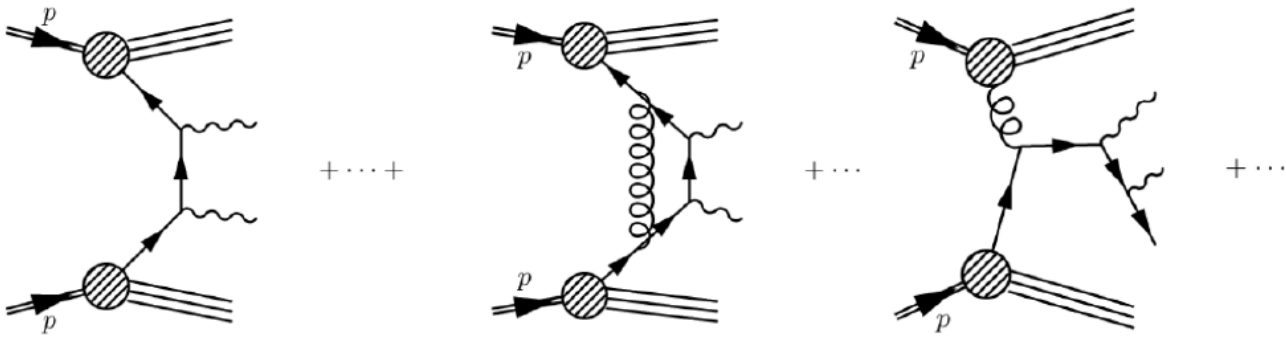

H $\to \gamma\gamma$ ($< 1\%$) and new phenomena (?)

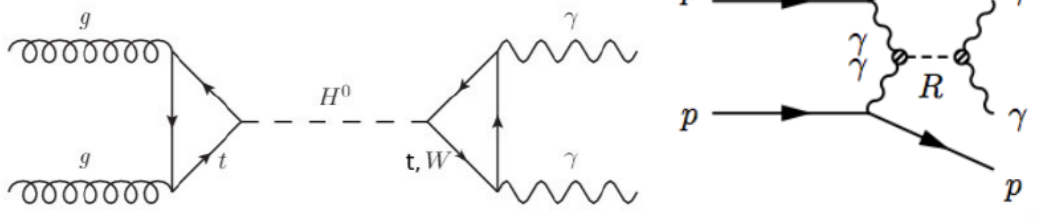

From collision data to xsec measurements

Integrated fiducial cross section and **differential cross section measurements** with respect to observables of interest $\mathcal{O}$:

fiducial $\rightarrow$ *restricted to the phase space with highest detector sensitivity (no extrapolation).*

$$\sigma_{\text{fid}} = \frac{\mathbf{N_{data}} - \mathbf{N_{bkg}}}{\epsilon_{\text{trig}} \cdot \mathbf{C_{total}} \cdot \mathcal{L}} \quad , \quad \frac{d\sigma_i}{d\mathcal{O}} = \frac{N_{data,i} - N_{bkg,i}}{\Delta\mathcal{O} \cdot \epsilon_{trig} \cdot C_{total,i} \cdot \mathcal{L}} \quad \textit{with } i = [\mathcal{O}_1, \mathcal{O}_2].$$

From collision data to xsec measurements

Integrated fiducial cross section and **differential cross section measurements** with respect to observables of interest $\mathcal{O}$:

fiducial $\rightarrow$ *restricted to the phase space with highest detector sensitivity (no extrapolation).*

$$\sigma_{\mathbf{fid}} = \frac{\boxed{\mathbf{N_{data}}} - \mathbf{N_{bkg}}}{\epsilon_{\mathbf{trig}} \cdot \mathbf{C_{total}} \cdot \mathcal{L}} \quad , \quad \frac{d\sigma_i}{d\mathcal{O}} = \frac{\boxed{N_{data,i}} - N_{bkg,i}}{\Delta\mathcal{O} \cdot \epsilon_{trig} \cdot C_{total,i} \cdot \mathcal{L}} \quad \textit{with } i = [\mathcal{O}_1, \mathcal{O}_2].$$

1. Selection of a data sample enriched in $pp \rightarrow \gamma\gamma + X$ final-states $(\mathbf{N_{data}})$.

From collision data to xsec measurements

Integrated fiducial cross section and **differential cross section measurements** with respect to observables of interest $\mathcal{O}$:

fiducial $\rightarrow$ *restricted to the phase space with highest detector sensitivity (no extrapolation).*

$$\sigma_{\mathbf{fid}} = \frac{\mathbf{N_{data}} - \boxed{\mathbf{N_{bkg}}}}{\epsilon_{\mathbf{trig}} \cdot \mathbf{C_{total}} \cdot \mathcal{L}} \quad , \quad \frac{d\sigma_i}{d\mathcal{O}} = \frac{N_{data,i} - \boxed{N_{bkg,i}}}{\Delta\mathcal{O} \cdot \epsilon_{trig} \cdot C_{total,i} \cdot \mathcal{L}} \quad \textit{with } i = [\mathcal{O}_1, \mathcal{O}_2].$$

1. Selection of a data sample enriched in $pp \rightarrow \gamma\gamma + X$ final-states **($\mathbf{N_{data}}$)**.

2. Subtraction of the remaining background present in the sample **($\mathbf{N_{bkg}}$)**.

   $\rightarrow$ *Based on data as much as possible, critical part on the analysis.*

From collision data to xsec measurements

Integrated fiducial cross section and **differential cross section measurements** with respect to observables of interest $\mathcal{O}$:

fiducial $\rightarrow$ *restricted to the phase space with highest detector sensitivity (no extrapolation).*

$$\sigma_{\text{fid}} = \frac{\mathbf{N_{data} - N_{bkg}}}{\boxed{\epsilon_{\text{trig}} \cdot \mathbf{C_{total}} \cdot \mathcal{L}}} \quad , \quad \frac{d\sigma_i}{d\mathcal{O}} = \frac{N_{data,i} - N_{bkg,i}}{\Delta\mathcal{O} \cdot \boxed{\epsilon_{trig} \cdot C_{total,i} \cdot \mathcal{L}}} \quad \text{with } i = [\mathcal{O}_1, \mathcal{O}_2].$$

1. Selection of a data sample enriched in $pp \rightarrow \gamma\gamma + X$ final-states $(\mathbf{N_{data}})$.

2. Subtraction of the remaining background present in the sample $(\mathbf{N_{bkg}})$.

   $\rightarrow$ *Based on data as much as possible, critical part on the analysis.*

3. Corrections related to detector inefficiencies and resolution $(\epsilon_{\text{trig.}}.\mathbf{C_{total}})$, and normalization to the integrated luminosity $(\mathcal{L})$.

From collision data to xsec measurements

Integrated fiducial cross section and **differential cross section measurements** with respect to observables of interest $\mathcal{O}$:

fiducial $\rightarrow$ *restricted to the phase space with highest detector sensitivity (no extrapolation).*

$$\sigma_{\text{fid}} = \frac{\mathbf{N_{data}} - \mathbf{N_{bkg}}}{\epsilon_{\text{trig}} \cdot \mathbf{C_{total}} \cdot \mathcal{L}} \quad , \quad \boxed{\frac{d\sigma_i}{d\mathcal{O}}} = \frac{N_{data,i} - N_{bkg,i}}{\boxed{\Delta\mathcal{O}} \cdot \epsilon_{trig} \cdot C_{total,i} \cdot \mathcal{L}} \quad \textit{with } i = [\mathcal{O}_1, \mathcal{O}_2].$$

1. Selection of a data sample enriched in $pp \rightarrow \gamma\gamma + X$ final-states **($\mathbf{N_{data}}$).**

2. Subtraction of the remaining background present in the sample **($\mathbf{N_{bkg}}$).**

   $\rightarrow$ *Based on data as much as possible, critical part on the analysis.*

3. Corrections related to detector inefficiencies and resolution **($\epsilon_{\text{trig.}}.\mathbf{C_{total}}$),** and normalization to the integrated luminosity **($\mathcal{L}$).**

   – **6 observables measured,** $\mathcal{O} = m_{\gamma\gamma}$, $|\cos\theta^*_\eta|$, $p_{\mathrm{T},\gamma\gamma}$, $\Delta\phi_{\gamma\gamma}$, a_{T}, ϕ^*_η.

From collision data to xsec measurements

Integrated fiducial cross section and **differential cross section measurements** with respect to observables of interest $\mathcal{O}$:

fiducial $\rightarrow$ *restricted to the phase space with highest detector sensitivity (no extrapolation).*

$$\sigma_{\text{fid}} = \frac{\mathbf{N_{data}} - \mathbf{N_{bkg}}}{\epsilon_{\text{trig}} \cdot \mathbf{C_{total}} \cdot \mathcal{L}} \quad , \quad \boxed{\frac{d\sigma_i}{d\mathcal{O}}} = \frac{N_{data,i} - N_{bkg,i}}{\boxed{\Delta\mathcal{O}} \cdot \epsilon_{trig} \cdot C_{total,i} \cdot \mathcal{L}} \quad \textit{with } i = [\mathcal{O}_1, \mathcal{O}_2].$$

1. Selection of a data sample enriched in $pp \rightarrow \gamma\gamma + X$ final-states **($\mathbf{N_{data}}$).**

2. Subtraction of the remaining background present in the sample **($\mathbf{N_{bkg}}$).**

   $\rightarrow$ *Based on data as much as possible, critical part on the analysis.*

3. Corrections related to detector inefficiencies and resolution **(ϵ_{trig}.$\mathbf{C_{total}}$)**, and normalization to the integrated luminosity **($\mathcal{L}$).**

   – **6 observables measured,** $\mathcal{O} = \boxed{m_{\gamma\gamma},\ |\cos\theta^*_\eta|}$, $p_{\mathrm{T},\gamma\gamma}$, $\Delta\phi_{\gamma\gamma}$, a_{T}, ϕ^*_η.

Variables of interest for new physics searches (resonances, spin).

From collision data to xsec measurements

Integrated fiducial cross section and **differential cross section measurements** with respect to observables of interest $\mathcal{O}$:

fiducial $\rightarrow$ *restricted to the phase space with highest detector sensitivity (no extrapolation).*

$$\sigma_{\text{fid}} = \frac{\mathbf{N_{data}} - \mathbf{N_{bkg}}}{\epsilon_{\text{trig}} \cdot \mathbf{C_{total}} \cdot \mathcal{L}} \quad , \quad \boxed{\frac{d\sigma_i}{d\mathcal{O}}} = \frac{N_{data,i} - N_{bkg,i}}{\boxed{\Delta\mathcal{O}} \cdot \epsilon_{trig} \cdot C_{total,i} \cdot \mathcal{L}} \quad \textit{with } i = [\mathcal{O}_1, \mathcal{O}_2].$$

1. Selection of a data sample enriched in $pp \rightarrow \gamma\gamma + X$ final-states **($\mathbf{N_{data}}$).**

2. Subtraction of the remaining background present in the sample **($\mathbf{N_{bkg}}$).**

   $\rightarrow$ *Based on data as much as possible, critical part on the analysis.*

3. Corrections related to detector inefficiencies and resolution **(ϵ_{trig}..$\mathbf{C_{total}}$)**, and normalization to the integrated luminosity **($\mathcal{L}$).**

   – **6 observables measured,** $\mathcal{O} = m_{\gamma\gamma}$, $|\cos\theta^*_\eta|$, $\boxed{p_{\mathrm{T},\gamma\gamma},\ \Delta\phi_{\gamma\gamma}}$, a_{T}, ϕ^*_η.

Sensitive to higher orders ($p_{\mathrm{T},\gamma\gamma} > 0, \Delta\phi_{\gamma\gamma} < \pi$) and QCD IR ($p_{\mathrm{T},\gamma\gamma} \simeq 0, \Delta\phi_{\gamma\gamma} \simeq \pi$).

From collision data to xsec measurements

Integrated fiducial cross section and **differential cross section measurements** with respect to observables of interest $\mathcal{O}$:

fiducial $\rightarrow$ *restricted to the phase space with highest detector sensitivity (no extrapolation).*

$$\sigma_{\text{fid}} = \frac{\mathbf{N_{data}} - \mathbf{N_{bkg}}}{\epsilon_{\text{trig}} \cdot \mathbf{C_{total}} \cdot \mathcal{L}} \quad , \quad \boxed{\frac{d\sigma_i}{d\mathcal{O}}} = \frac{N_{data,i} - N_{bkg,i}}{\boxed{\Delta\mathcal{O}} \cdot \epsilon_{trig} \cdot C_{total,i} \cdot \mathcal{L}} \quad \textit{with } i = [\mathcal{O}_1, \mathcal{O}_2].$$

1. Selection of a data sample enriched in $pp \rightarrow \gamma\gamma + X$ final-states **($\mathbf{N_{data}}$).**

2. Subtraction of the remaining background present in the sample **($\mathbf{N_{bkg}}$).**

   $\rightarrow$ *Based on data as much as possible, critical part on the analysis.*

3. Corrections related to detector inefficiencies and resolution **(ϵ_{trig}.$\mathbf{C_{total}}$)**, and normalization to the integrated luminosity **($\mathcal{L}$).**

   – **6 observables measured,** $\mathcal{O} = m_{\gamma\gamma}$, $|\cos\theta^*_\eta|$, $p_{\mathrm{T},\gamma\gamma}$, $\Delta\phi_{\gamma\gamma}$, $\boxed{a_{\mathrm{T}}, \phi^*_\eta}$.

2 new variables to probe precisely QCD infrared emissions (see next slide).

New variables studied at $\sqrt{s} = 8$ TeV

Nucl. Instrum. Meth. A **602** (2009) 432437

Eur. Phys. J. C **71** (2011) 1600

- a_{T}: $\perp$ projection of $p_{\mathrm{T},\gamma\gamma}$

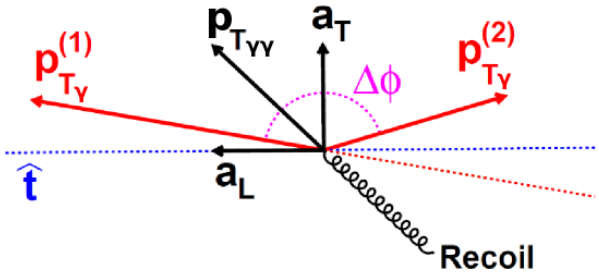

New variables studied at $\sqrt{s} = 8$ TeV

Nucl. Instrum. Meth. A **602** (2009) 432437

Eur. Phys. J. C **71** (2011) 1600

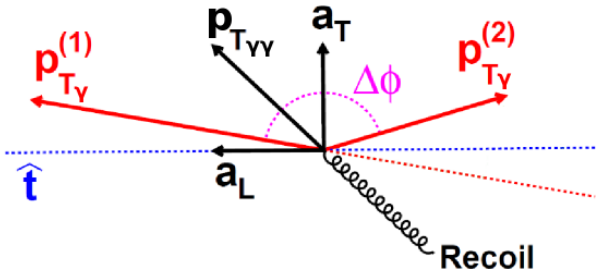

- a_T: $\perp$ projection of $p_{T,\gamma\gamma}$
- $|\cos\theta^*_\eta| = \tanh\left(\frac{|\Delta\eta_{\gamma\gamma}|}{2}\right)$
- $\phi^*_\eta = \tan\left(\frac{\pi - \Delta\phi_{\gamma\gamma}}{2}\right)\sin\theta^*_\eta$

$\rightarrow$ use of a particular reference frame to improve resolution of $|\cos\theta^*_\eta|$ and ϕ^*_η.

New variables studied at $\sqrt{s} = 8$ TeV

Nucl. Instrum. Meth. A **602** (2009) 432437

Eur. Phys. J. C **71** (2011) 1600

- a_{T}: $\perp$ projection of $p_{\mathrm{T},\gamma\gamma}$
- $|\cos\theta^*_\eta| = \tanh\left(\frac{|\Delta\eta_{\gamma\gamma}|}{2}\right)$
- $\phi^*_\eta = \tan\left(\frac{\pi - \Delta\phi_{\gamma\gamma}}{2}\right)\sin\theta^*_\eta$

$\rightarrow$ use of a particular reference frame to improve resolution of $|\cos\theta^*_\eta|$ and ϕ^*_η.

$\rightarrow$ **High resolution of a_{T} and ϕ^*_η, especially when photons almost back-to-back.**

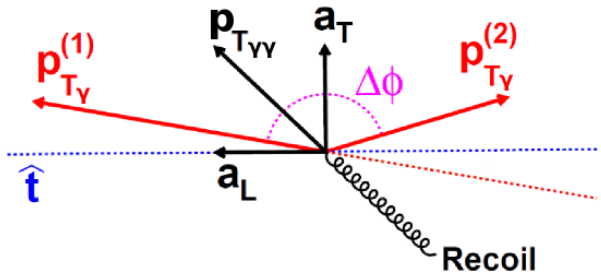

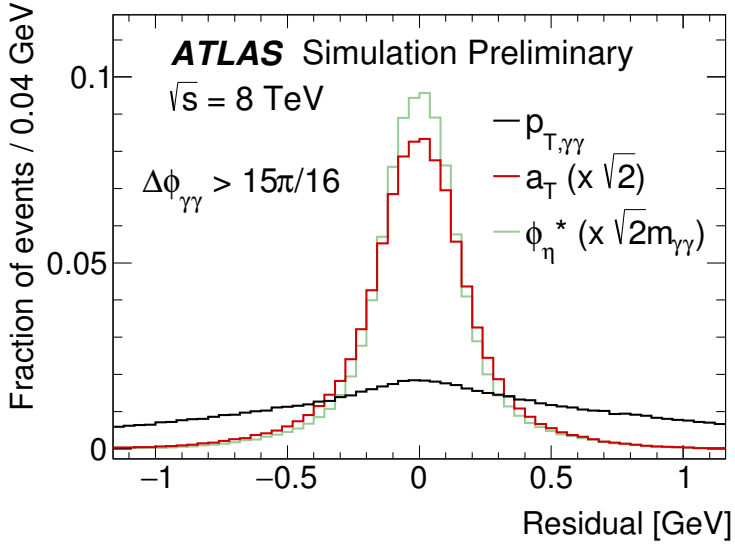

New variables studied at $\sqrt{s} = 8$ TeV

Nucl. Instrum. Meth. A **602** (2009) 432437

Eur. Phys. J. C **71** (2011) 1600

- a_{T}: $\perp$ projection of $p_{\mathrm{T},\gamma\gamma}$
- $|\cos\theta^*_\eta| = \tanh\left(\frac{|\Delta\eta_{\gamma\gamma}|}{2}\right)$
- $\phi^*_\eta = \tan\left(\frac{\pi - \Delta\phi_{\gamma\gamma}}{2}\right)\sin\theta^*_\eta$

$\rightarrow$ use of a particular reference frame to improve resolution of $|\cos\theta^*_\eta|$ and ϕ^*_η.

$\rightarrow$ **High resolution of a_{T} and ϕ^*_η, especially when photons almost back-to-back.**

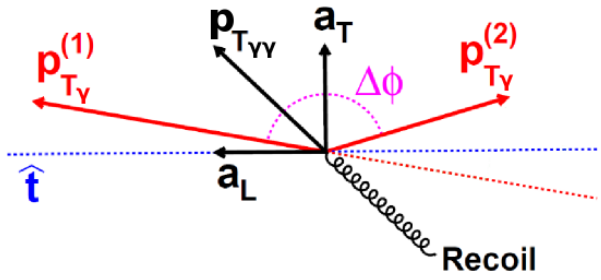

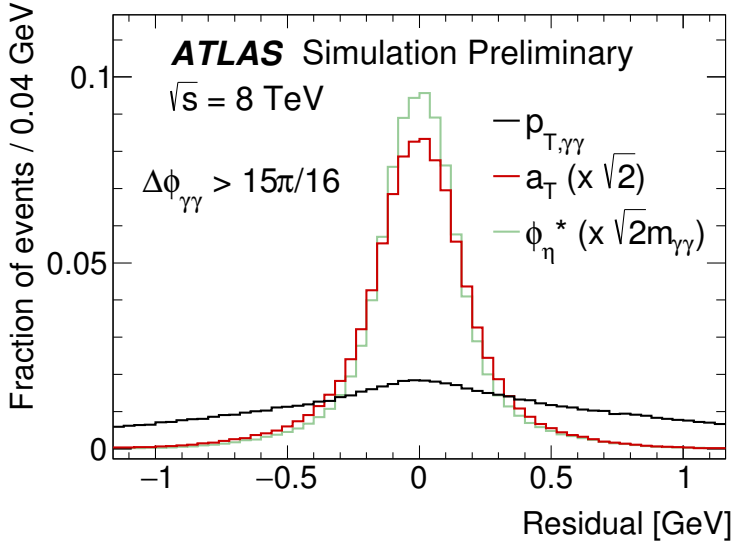

ϕ^*_η recently measured by ATLAS for Drell-Yan (dominated by $q\bar{q}$ initial states),
Eur. Phys. J. C **76** (5), 1-61 (2016)

Changes/Improvements compared to 7 TeV

Previous ATLAS $\gamma\gamma + X$ measurement

JHEP **01** (2013) 086

- $\sqrt{s} = 7$ TeV, 4.7 fb^{-1}
- $m_{\gamma\gamma}$, $p_{\mathrm{T},\gamma\gamma}$, $\Delta\phi_{\gamma\gamma}$, $\cos\theta^*_{\mathrm{CS}}$

New ATLAS $\gamma\gamma + X$ measurement

preliminary results

- $\sqrt{s} = 8$ TeV, 20.2 fb^{-1}
- $m_{\gamma\gamma}$, $p_{\mathrm{T},\gamma\gamma}$, $\Delta\phi_{\gamma\gamma}$, $|\cos\theta^*_\eta|$, a_{T}, ϕ^*_η.

Changes/Improvements compared to 7 TeV

Previous ATLAS $\gamma\gamma + X$ measurement

JHEP **01** (2013) 086

- $\sqrt{s} = 7$ TeV, 4.7 fb^{-1}
- $m_{\gamma\gamma}$, $p_{\mathrm{T},\gamma\gamma}$, $\Delta\phi_{\gamma\gamma}$, $\cos\theta^*_{\mathrm{CS}}$
- $< \mu >= 9.1$ (average pileup)

New ATLAS $\gamma\gamma + X$ measurement

preliminary results

- $\sqrt{s} = 8$ TeV, 20.2 fb^{-1}
- $m_{\gamma\gamma}$, $p_{\mathrm{T},\gamma\gamma}$, $\Delta\phi_{\gamma\gamma}$, $|\cos\theta^*_\eta|$, a_{T}, ϕ^*_η.
- $< \mu >= 20.7$

Changes/Improvements compared to 7 TeV

Previous ATLAS $\gamma\gamma + X$ measurement

JHEP **01** (2013) 086

- $\sqrt{s} = 7$ TeV, 4.7 fb^{-1}
- $m_{\gamma\gamma}$, $p_{\mathrm{T},\gamma\gamma}$, $\Delta\phi_{\gamma\gamma}$, $\cos\theta^*_{\mathrm{CS}}$
- $< \mu >= 9.1$ (average pileup)
- $\mathrm{E}^{\gamma}_{\mathrm{T},1} > 25$ GeV, $\mathrm{E}^{\gamma}_{\mathrm{T},2} > 22$ GeV

New ATLAS $\gamma\gamma + X$ measurement

preliminary results

- $\sqrt{s} = 8$ TeV, 20.2 fb^{-1}
- $m_{\gamma\gamma}$, $p_{\mathrm{T},\gamma\gamma}$, $\Delta\phi_{\gamma\gamma}$, $|\cos\theta^*_{\eta}|$, a_{T}, ϕ^*_{η}.
- $< \mu >= 20.7$
- $\mathrm{E}^{\gamma}_{\mathrm{T},1} > 40$ GeV, $\mathrm{E}^{\gamma}_{\mathrm{T},2} > 30$ GeV

Changes/Improvements compared to 7 TeV

Previous ATLAS $\gamma\gamma + X$ measurement

JHEP **01** (2013) 086

- $\sqrt{s} = 7$ TeV, 4.7 fb^{-1}
- $m_{\gamma\gamma}$, $p_{\mathrm{T},\gamma\gamma}$, $\Delta\phi_{\gamma\gamma}$, $\cos\theta^*_{\mathrm{CS}}$
- $< \mu >= 9.1$ (average pileup)
- $\mathrm{E}^{\gamma}_{\mathrm{T},1} > 25$ GeV, $\mathrm{E}^{\gamma}_{\mathrm{T},2} > 22$ GeV
- Calorimeter isolation requirement

New ATLAS $\gamma\gamma + X$ measurement

preliminary results

- $\sqrt{s} = 8$ TeV, 20.2 fb^{-1}
- $m_{\gamma\gamma}$, $p_{\mathrm{T},\gamma\gamma}$, $\Delta\phi_{\gamma\gamma}$, $|\cos\theta^*_{\eta}|$, a_{T}, ϕ^*_{η}.
- $< \mu >= 20.7$
- $\mathrm{E}^{\gamma}_{\mathrm{T},1} > 40$ GeV, $\mathrm{E}^{\gamma}_{\mathrm{T},2} > 30$ GeV
- Calo. + track isolation requirement

Changes/Improvements compared to 7 TeV

Previous ATLAS $\gamma\gamma$ + X measurement

JHEP **01** (2013) 086

- $\sqrt{s} = 7$ TeV, 4.7 fb^{-1}
- $m_{\gamma\gamma}$, $p_{\mathrm{T},\gamma\gamma}$, $\Delta\phi_{\gamma\gamma}$, $\cos\theta^*_{\mathrm{CS}}$
- $< \mu >= 9.1$ (average pileup)
- $\mathrm{E}^{\gamma}_{\mathrm{T},1} > 25$ GeV, $\mathrm{E}^{\gamma}_{\mathrm{T},2} > 22$ GeV
- Calorimeter isolation requirement
- Data-driven background subtraction

New ATLAS $\gamma\gamma$ + X measurement

preliminary results

- $\sqrt{s} = 8$ TeV, 20.2 fb^{-1}
- $m_{\gamma\gamma}$, $p_{\mathrm{T},\gamma\gamma}$, $\Delta\phi_{\gamma\gamma}$, $|\cos\theta^*_{\eta}|$, a_{T}, ϕ^*_{η}.
- $< \mu >= 20.7$
- $\mathrm{E}^{\gamma}_{\mathrm{T},1} > 40$ GeV, $\mathrm{E}^{\gamma}_{\mathrm{T},2} > 30$ GeV
- Calo. + track isolation requirement
- Improved data-driven subtraction

Changes/Improvements compared to 7 TeV

Previous ATLAS $\gamma\gamma$ + X measurement

JHEP **01** (2013) 086

- $\sqrt{s} = 7$ TeV, 4.7 fb^{-1}
- $m_{\gamma\gamma}$, $p_{\mathrm{T},\gamma\gamma}$, $\Delta\phi_{\gamma\gamma}$, $\cos\theta^*_{\mathrm{CS}}$
- $< \mu >= 9.1$ (average pileup)
- $\mathrm{E}^{\gamma}_{\mathrm{T},1} > 25$ GeV, $\mathrm{E}^{\gamma}_{\mathrm{T},2} > 22$ GeV
- Calorimeter isolation requirement
- Data-driven background subtraction
- **Typical systematic unc. $\pm$ 7-8%**

New ATLAS $\gamma\gamma$ + X measurement

preliminary results

- $\sqrt{s} = 8$ TeV, 20.2 fb^{-1}
- $m_{\gamma\gamma}$, $p_{\mathrm{T},\gamma\gamma}$, $\Delta\phi_{\gamma\gamma}$, $|\cos\theta^*_{\eta}|$, a_{T}, ϕ^*_{η}.
- $< \mu >= 20.7$
- $\mathrm{E}^{\gamma}_{\mathrm{T},1} > 40$ GeV, $\mathrm{E}^{\gamma}_{\mathrm{T},2} > 30$ GeV
- Calo. + track isolation requirement
- Improved data-driven subtraction
- **Typical syst. uncertainty $\pm$ 4-5%**

Event selection

- At least two reconstructed and well-separated photons ($\Delta R_{\gamma\gamma} > 0.4$).
- $E_{T,1}^{\gamma} > 40$ GeV, $E_{T,2}^{\gamma} > 30$ GeV
- $|\eta^{\gamma}| < 1.37$ or $1.56 < |\eta^{\gamma}| < 2.37$

Event selection

- At least two reconstructed and well-separated photons ($\Delta R_{\gamma\gamma} > 0.4$).
- $E^{\gamma}_{T,1} > 40$ GeV, $E^{\gamma}_{T,2} > 30$ GeV
- $|\eta^{\gamma}| < 1.37$ or $1.56 < |\eta^{\gamma}| < 2.37$
- Photon energy depositions in the calorimeter must match expectations for photon-initiated showers **(a.k.a. identification)**.

Eur. Phys. J. C **76** (2016) 666

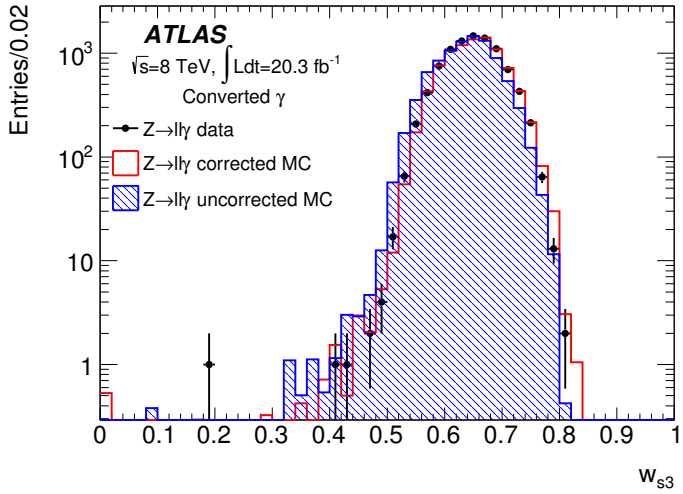

Event selection

- At least two reconstructed and well-separated photons ($\Delta R_{\gamma\gamma} > 0.4$).
- $E^{\gamma}_{T,1} > 40$ GeV, $E^{\gamma}_{T,2} > 30$ GeV
- $|\eta^{\gamma}| < 1.37$ or $1.56 < |\eta^{\gamma}| < 2.37$
- Photon energy depositions in the calorimeter must match expectations for photon-initiated showers **(a.k.a. identification)**.

Eur. Phys. J. C **76** (2016) 666

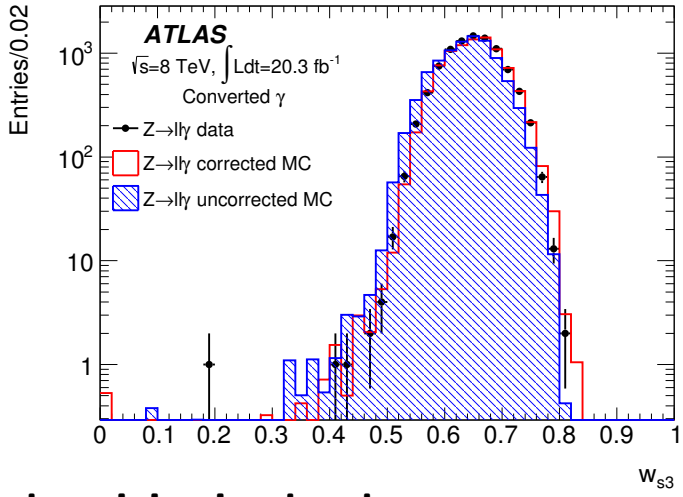

- **The two photons must be isolated from additional activity in the detector.**

$\boxed{p_{\mathrm{T}}^{\mathrm{iso}}(\Delta R = 0.2) < 2.6\ \mathrm{GeV}}$ (*) and $\boxed{E_{\mathrm{T}}^{\mathrm{iso}}(\Delta R = 0.4) < 6\ \mathrm{GeV}}$ (**)

(*) Scalar sum of the $p_{\mathrm{T}} > 1$ GeV of tracks within a cone of size $\Delta R = 0.2$ around the photon candidate.

(**) Scalar sum of the $E_{\mathrm{T}} > 0$ GeV of topological clusters within a cone of size $\Delta R = 0.4$.

Event selection

- At least two reconstructed and well-separated photons ($\Delta R_{\gamma\gamma} > 0.4$).
- $E^{\gamma}_{T,1} > 40$ GeV, $E^{\gamma}_{T,2} > 30$ GeV
- $|\eta^{\gamma}| < 1.37$ or $1.56 < |\eta^{\gamma}| < 2.37$
- Photon energy depositions in the calorimeter must match expectations for photon-initiated showers **(a.k.a. identification)**.

Eur. Phys. J. C **76** (2016) 666

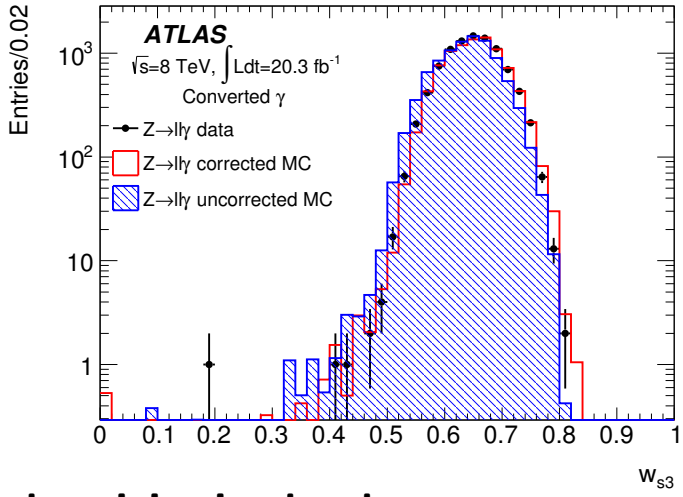

- **The two photons must be isolated from additional activity in the detector.**

$\boxed{p_{\mathrm{T}}^{\mathrm{iso}}(\Delta R = 0.2) < 2.6\ \mathrm{GeV}}$ (*) and $\boxed{E_{\mathrm{T}}^{\mathrm{iso}}(\Delta R = 0.4) < 6\ \mathrm{GeV}}$ (**)

(*) Scalar sum of the $p_{\mathrm{T}} > 1$ GeV of tracks within a cone of size $\Delta R = 0.2$ around the photon candidate.

(**) Scalar sum of the $E_{\mathrm{T}} > 0$ GeV of topological clusters within a cone of size $\Delta R = 0.4$.

- **Typical composition of the selected sample:**
  - 75% signal events
  - **22% background events from misidentified jets**
  - 3% background events from misidentified electrons

main background. (at high p_{T}, $\theta \to 0$)

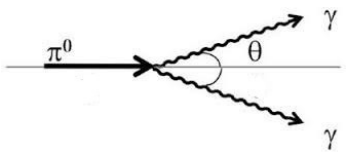

Event selection

- At least two reconstructed and well-separated photons ($\Delta R_{\gamma\gamma} > 0.4$).
- $E^{\gamma}_{T,1} > 40$ GeV, $E^{\gamma}_{T,2} > 30$ GeV
- $|\eta^{\gamma}| < 1.37$ or $1.56 < |\eta^{\gamma}| < 2.37$
- Photon energy depositions in the calorimeter must match expectations for photon-initiated showers **(a.k.a. identification)**.

Eur. Phys. J. C **76** (2016) 666

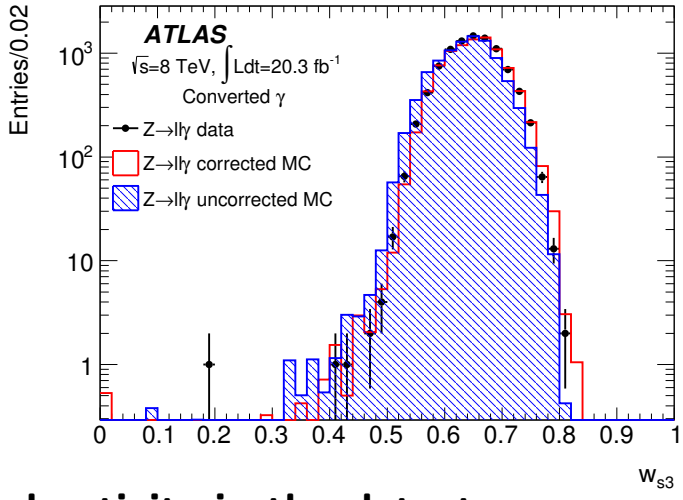

- **The two photons must be isolated from additional activity in the detector.**

$$\boxed{p_{\mathrm{T}}^{\mathrm{iso}}(\Delta R = 0.2) < 2.6\ \mathrm{GeV}}\ (*) \qquad \text{and} \qquad \boxed{E_{\mathrm{T}}^{\mathrm{iso}}(\Delta R = 0.4) < 6\ \mathrm{GeV}}\ (**)$$

(*) Scalar sum of the $p_{\mathrm{T}} > 1$ GeV of tracks within a cone of size $\Delta R = 0.2$ around the photon candidate.

(**) Scalar sum of the $E_{\mathrm{T}} > 0$ GeV of topological clusters within a cone of size $\Delta R = 0.4$.

- **Typical composition of the selected sample:**
  - 75% signal events
  - **22% background events from misidentified jets**
  - 3% background events from misidentified electrons

main background. (at high p_{T}, $\theta \to 0$)

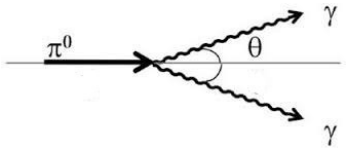

Subtraction of the remaining background very challenging (non-pert. QCD).

Subtraction of the remaining background

- Two methods giving compatible results and validated using pseudo-data generated with known signal and background composition are used.

Subtraction of the remaining background

– Two methods giving compatible results and validated using pseudo-data generated with known signal and background composition are used.

Template fit method **(used for final results)**

- 2D fit to ($E_{\mathrm{T},1}^{\mathrm{iso}}$, $E_{\mathrm{T},2}^{\mathrm{iso}}$) distribution in signal region (SR).

Subtraction of the remaining background

– Two methods giving compatible results and validated using pseudo-data generated with known signal and background composition are used.

Template fit method **(used for final results)**

- 2D fit to ($E_{\mathrm{T},1}^{\mathrm{iso}}$, $E_{\mathrm{T},2}^{\mathrm{iso}}$) distribution in signal region (SR).
- 1 signal + 4 background components included.

Subtraction of the remaining background

– Two methods giving compatible results and validated using pseudo-data generated with known signal and background composition are used.

Template fit method **(used for final results)**

- 2D fit to ($E_{\mathrm{T},1}^{\mathrm{iso}}$, $E_{\mathrm{T},2}^{\mathrm{iso}}$) distribution in signal region (SR).
- 1 signal + 4 background components included.
- Most sensitive to the modeling of isolation for signal
  now constrained with inclusive γ data

Subtraction of the remaining background

– Two methods giving compatible results and validated using pseudo-data generated with known signal and background composition are used.

Template fit method **(used for final results)**

- 2D fit to ($E_{\mathrm{T},1}^{\mathrm{iso}}$, $E_{\mathrm{T},2}^{\mathrm{iso}}$) distribution in signal region (SR).
- 1 signal + 4 background components included.
- Most sensitive to the modeling of isolation for signal
  now constrained with inclusive γ data

$E_{\mathrm{T},1}^{\mathrm{iso}}$ in the integrated signal region after fit

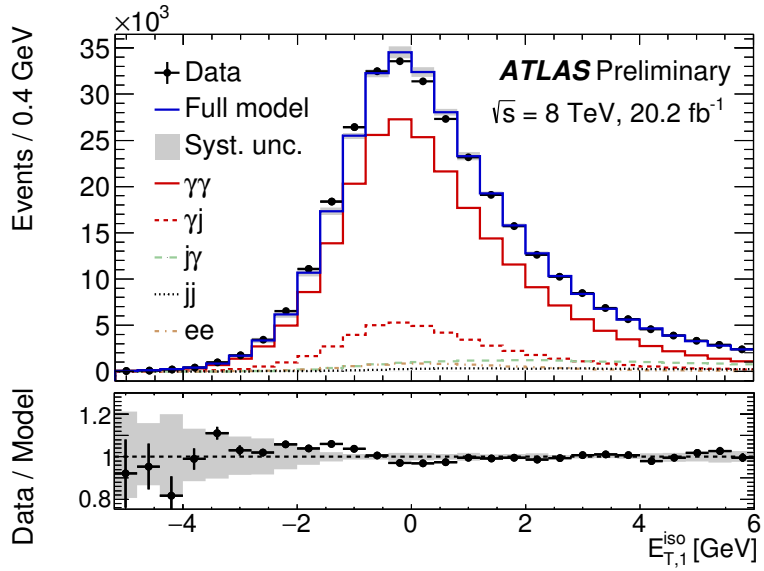

Subtraction of the remaining background

– Two methods giving compatible results and validated using pseudo-data generated with known signal and background composition are used.

Template fit method (used for final results)

- 2D fit to ($E_{\mathrm{T},1}^{\mathrm{iso}}$, $E_{\mathrm{T},2}^{\mathrm{iso}}$) distribution in signal region (SR).
- 1 signal + 4 background components included.
- Most sensitive to the modeling of isolation for signal now constrained with inclusive γ data

$E_{\mathrm{T},1}^{\mathrm{iso}}$ in the integrated signal region after fit

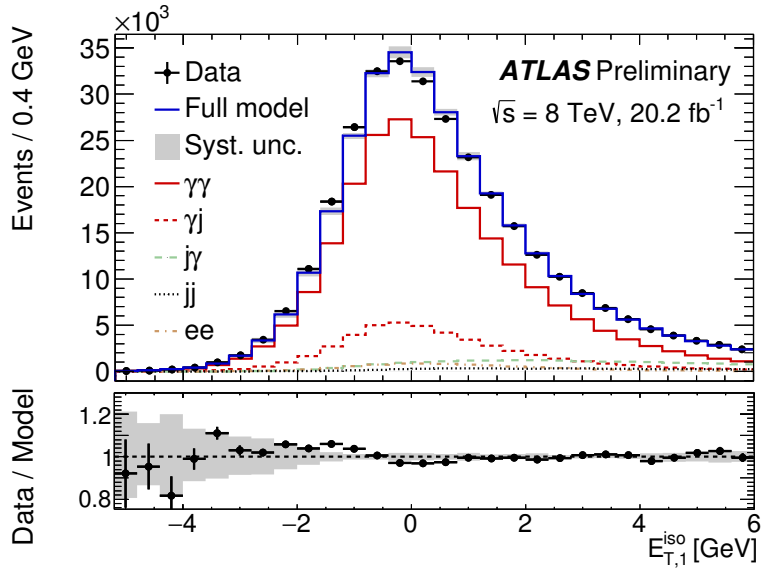

Matrix method (used as a cross-check)

- Solve a linear system based on number of isolated and non-isolated events.
- Use of data control regions in a wide range of isolation energy.
- Most sensitive to shower shapes / isolation energy correlations.

Sample composition

- Background subtraction performed in the integrated signal region and in each bin.

Sample composition

- Background subtraction performed in the integrated signal region and in each bin.
- Many improvements in the background subtraction method.

Sample composition

- Background subtraction performed in the integrated signal region and in each bin.
- Many improvements in the background subtraction method.
- Correlation between the two methods evaluated ($\simeq 25\%$). $\boxed{\sim 1\sigma \text{ compatibility}}$.

Sample composition

- Background subtraction performed in the integrated signal region and in each bin.
- Many improvements in the background subtraction method.
- Correlation between the two methods evaluated ($\simeq 25\%$). $\boxed{\sim 1\sigma \text{ compatibility}}$.

Integrated signal region

$\gamma\gamma$ event fraction $\pm$ syst. [%]

Template fit: $\mathbf{75.3}\ ^{+2.6}_{-2.8}$

Matrix: $\mathbf{73.9}\ ^{+3.1}_{-2.7}$

(statistical uncertainty $\sim 0.3\%$)

Bin-by-bin composition (template fit)

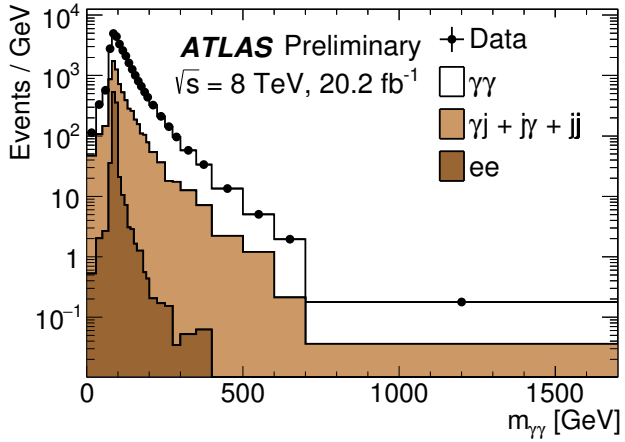

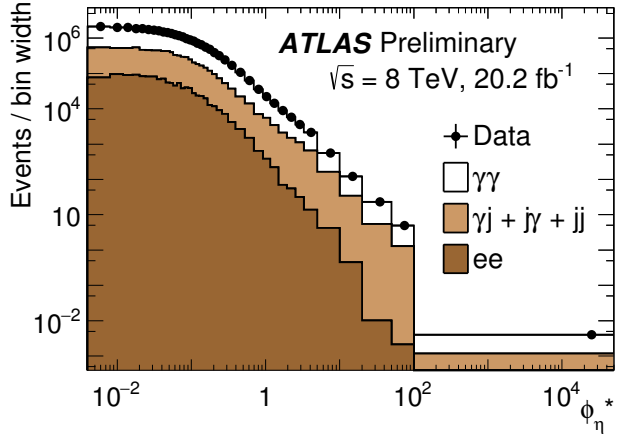

Unfolding and final uncertainties

– Cross-section measurements performed in a fiducial region at particle level close to the event selection.

Fiducial region at particle level

Leading γ	Subleading γ
$E_{\mathrm{T},1}^{\gamma} > 40$ GeV	$E_{\mathrm{T},2}^{\gamma} > 30$ GeV
$\lvert\eta^{\gamma}\rvert < 1.37$ or $1.56 < \lvert\eta^{\gamma}\rvert < 2.37$	
$\Delta R_{\gamma\gamma} > 0.4$	
$E_{\mathrm{T}}^{\mathrm{iso,part}}(\Delta R = 0.4) < 11$ GeV	
not originating from hadron/τ decays	

Unfolding and final uncertainties

- Cross-section measurements performed in a fiducial region at particle level close to the event selection.
- Use of an iterative Bayesian unfolding method to correct for detector resolution, reconstruction and selection efficiencies.

  $\rightarrow$ *at least 70% of the generated events are reconstructed in the same bin.*

Fiducial region at particle level

Leading γ	Subleading γ
$E_{\mathrm{T},1}^{\gamma} > 40$ GeV	$E_{\mathrm{T},2}^{\gamma} > 30$ GeV
$\lvert\eta^{\gamma}\rvert < 1.37$ or $1.56 < \lvert\eta^{\gamma}\rvert < 2.37$	
$\Delta R_{\gamma\gamma} > 0.4$	
$E_{\mathrm{T}}^{\mathrm{iso,part}}(\Delta R = 0.4) < 11$ GeV	
not originating from hadron/τ decays	

Unfolding and final uncertainties

- Cross-section measurements performed in a fiducial region at particle level close to the event selection.
- Use of an iterative Bayesian unfolding method to correct for detector resolution, reconstruction and selection efficiencies.

  $\rightarrow$ *at least 70% of the generated events are reconstructed in the same bin.*

Fiducial region at particle level

Leading γ	Subleading γ
$E_{\mathrm{T},1}^{\gamma} > 40$ GeV	$E_{\mathrm{T},2}^{\gamma} > 30$ GeV
$\lvert\eta^{\gamma}\rvert < 1.37$ or $1.56 < \lvert\eta^{\gamma}\rvert < 2.37$	
$\Delta R_{\gamma\gamma} > 0.4$	
$E_{\mathrm{T}}^{\mathrm{iso,part}}(\Delta R = 0.4) < 11$ GeV	
not originating from hadron/τ decays	

Main syst. uncertainties in the integrated fiducial cross section

Source of systematic uncertainty	Impact on $\sigma_{\mathrm{tot}}^{\mathrm{fid.}}$ [%]
Photon identification efficiency	± 2.5
Modeling of calorimeter isolation	± 2.0
Luminosity	± 1.9
Other sources combined (all $< 1.7\%$)	~ 2.8
Total	~ 4.7

Comparison to theoretical predictions

- 4 theoretical predictions generated:
  - **parton level, CT10 NLO:**
    DIPHOX (NLO), Eur. Phys. J. C **16** (2000)
    RESBOS (NLO+NNLL)*, Phys. Rev. D **76** (2007)

Comparison to theoretical predictions

- 4 theoretical predictions generated:
  - **parton level, CT10 NLO:**
    DIPHOX (NLO), Eur. Phys. J. C **16** (2000)
    RESBOS (NLO+NNLL)*, Phys. Rev. D **76** (2007)
  - **parton level, CT10 NNLO:**
    2γNNLO (NNLO), Phys. Rev. Lett. **108** (2012)

Comparison to theoretical predictions

- 4 theoretical predictions generated:
  - **parton level, CT10 NLO:**
    DIPHOX (NLO), Eur. Phys. J. C **16** (2000)
    RESBOS (NLO+NNLL)*, Phys. Rev. D **76** (2007)
  - **parton level, CT10 NNLO:**
    2γNNLO (NNLO), Phys. Rev. Lett. **108** (2012)
  - **particle level (parton shower), NNPDF3.0 NNLO:**
    SHERPA 2.2.1 (ME+PS)**, arXiv:1611.07226 (2016)

  * no theoretical uncertainties were provided.
  ** $\gamma\gamma + 0, 1$ parton at NLO, $\gamma\gamma + 2, 3$ parton at LO.

Comparison to theoretical predictions

- 4 theoretical predictions generated:
  - **parton level, CT10 NLO:**
    DIPHOX (NLO), Eur. Phys. J. C **16** (2000)
    RESBOS (NLO+NNLL)*, Phys. Rev. D **76** (2007)
  - **parton level, CT10 NNLO:**
    2γNNLO (NNLO), Phys. Rev. Lett. **108** (2012)
  - **particle level (parton shower), NNPDF3.0 NNLO:**
    SHERPA 2.2.1 (ME+PS)**, arXiv:1611.07226 (2016)

  * no theoretical uncertainties were provided.
  ** $\gamma\gamma + 0, 1$ parton at NLO, $\gamma\gamma + 2, 3$ parton at LO.

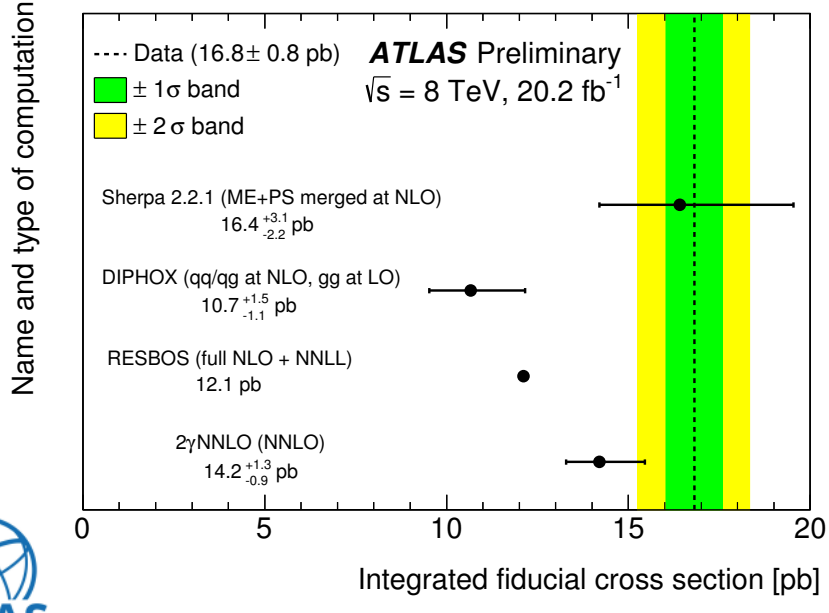

ϕ^*_η differential cross section measurement

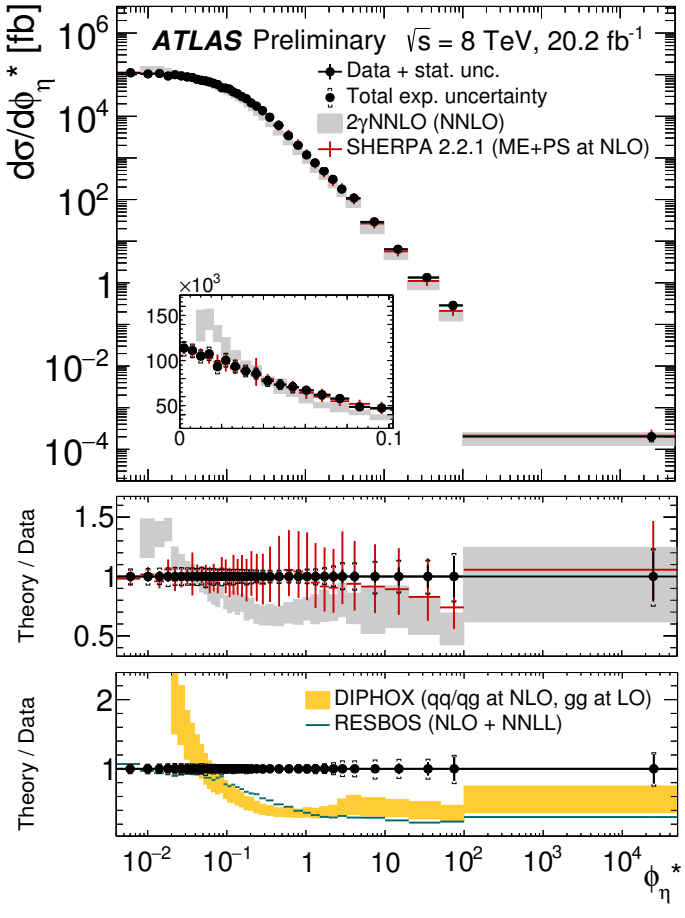

- DIPHOX, 2γNNLO: missing α_s corrections, fails at describing QCD infrared emissions.
- RESBOS: missing α_s corrections.
- SHERPA 2.2.1 is in good agreement.

More on data/theory comparisons

- **SHERPA 2.2.1 provides an improved description of the data** compared to all other computations considered for all observables.
- Theoretical uncertainties dominated by **scale variations** ($\sim$ 5–20%).
  (PDF uncertainties $\sim$ 2%)
- Parton-level computations corrected from non-perturbative effects, typically $< 5\%$.

$m_{\gamma\gamma}$ differential cross section measurement

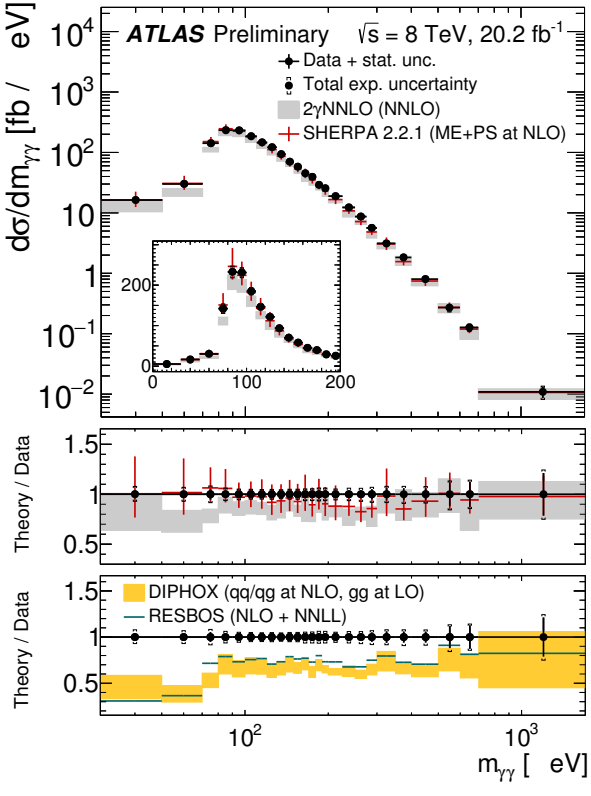

$\Delta\phi_{\gamma\gamma}$ differential cross section measurement

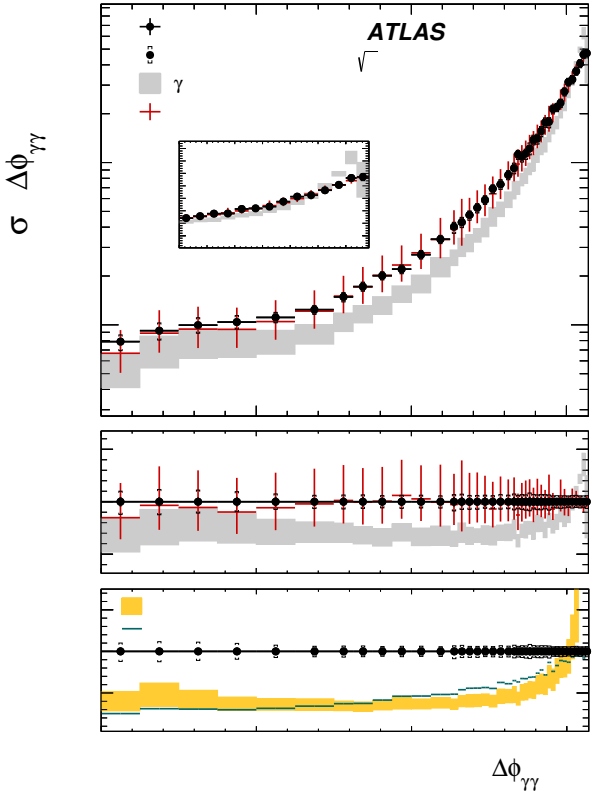

More on data/theory comparisons

- **SHERPA 2.2.1 provides an improved description of the data** compared to all other computations considered for all observables.
- Theoretical uncertainties dominated by **scale variations** ($\sim$ 5–20%).
  (PDF uncertainties $\sim$ 2%)
- Parton-level computations corrected from non-perturbative effects, typically $< 5\%$.

$p_{T,\gamma\gamma}$ differential cross section measurement

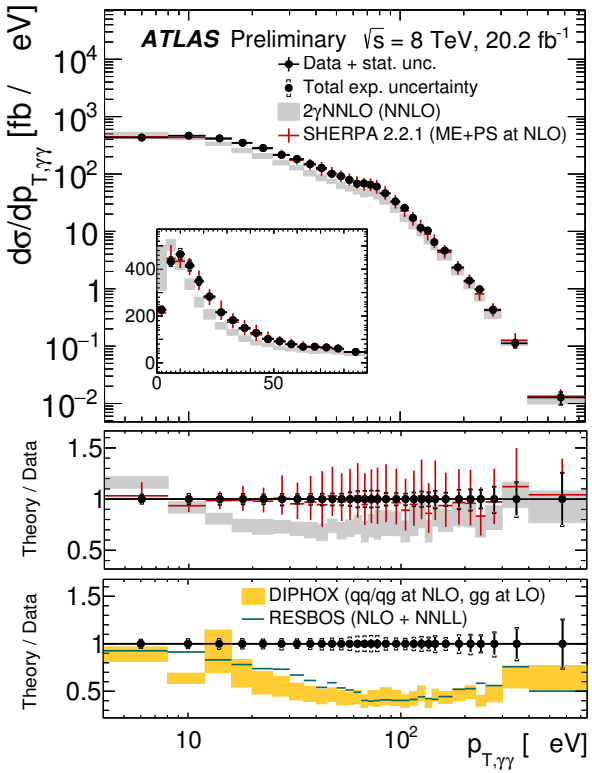

a_T differential cross section measurement

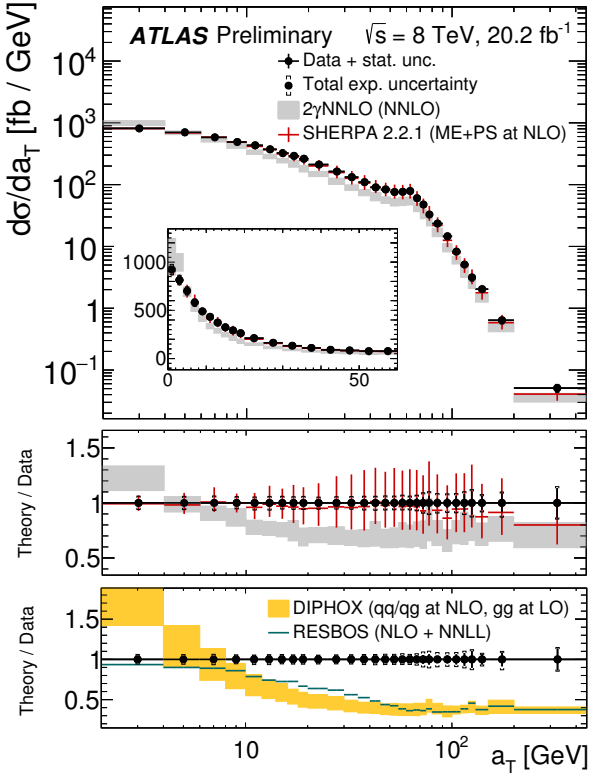

More on data/theory comparisons

- **SHERPA 2.2.1 provides an improved description of the data** compared to all other computations considered for all observables.
- Theoretical uncertainties dominated by **scale variations** ($\sim$ 5–20%).
  (PDF uncertainties $\sim$ 2%)
- Parton-level computations corrected from non-perturbative effects, typically $< 5\%$.

$|\cos\theta^*_\eta|$ differential cross section measurement

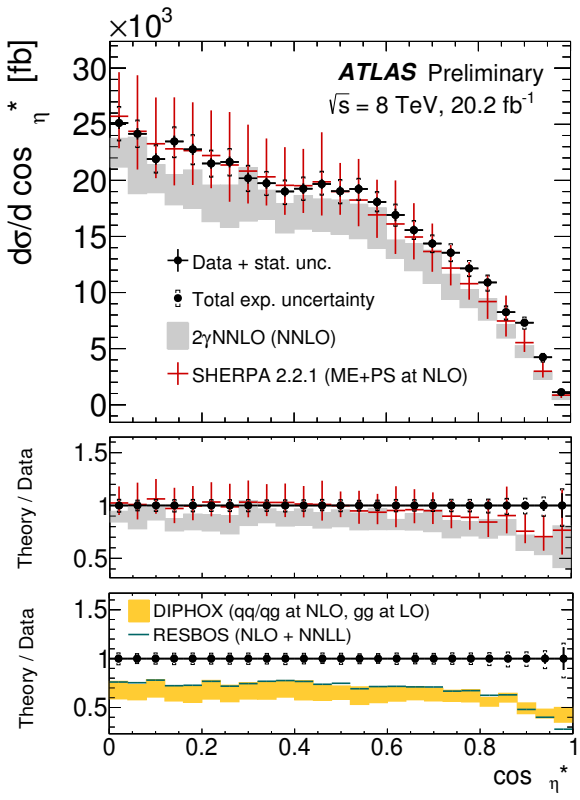

a_T differential cross section measurement

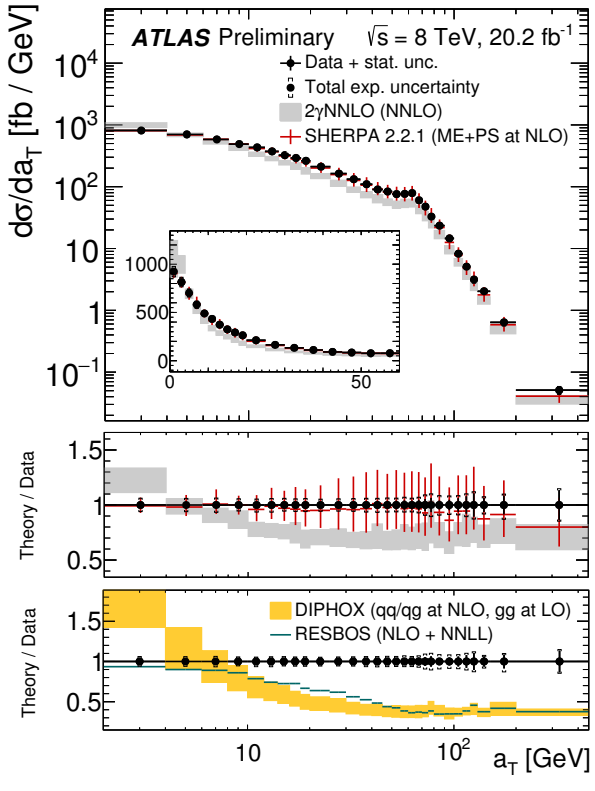

Summary

- ATLAS precision measurement of $\gamma\gamma$ final states in pp collisions at $\sqrt{s} = 8$ TeV

$$\sigma_{\text{tot}}^{\text{fid.}} = 16.8 \pm 0.1\ (\text{stat})\ \pm 0.7\ (\text{syst})\ \pm 0.3\ (\text{lumi})\ \text{pb} = 16.8 \pm 0.8\ \text{pb}$$

Summary

- ATLAS precision measurement of $\gamma\gamma$ final states in pp collisions at $\sqrt{s} = 8$ TeV

$$\sigma_{\text{tot}}^{\text{fid.}} = 16.8 \pm 0.1\ (\text{stat})\ \pm 0.7\ (\text{syst})\ \pm 0.3\ (\text{lumi})\ \text{pb} = 16.8 \pm 0.8\ \text{pb}$$

- Systematic uncertainties **decreased by up to a factor 2** w.r.t. the previous ATLAS measurement (7 TeV).

Summary

- ATLAS precision measurement of $\gamma\gamma$ final states in *pp* collisions at $\sqrt{s} = 8$ TeV

$$\sigma_{\text{tot}}^{\text{fid.}} = 16.8 \pm 0.1\ (\text{stat})\ \pm 0.7\ (\text{syst})\ \pm 0.3\ (\text{lumi})\ \text{pb} = 16.8 \pm 0.8\ \text{pb}$$

- Systematic uncertainties **decreased by up to a factor 2** w.r.t. the previous ATLAS measurement (7 TeV).
- **Precise probe of QCD infrared emissions** (a_{T}, ϕ_{η}^{*}), complementary to Drell-Yan.
  - **$\gamma\gamma$ originates from both $q\bar{q}$ and gg initial states.**
  - Important prerequisite for models aiming to describe the low q_{T} region in more complicated processes (e.g. coloured final states).

Summary

- ATLAS precision measurement of $\gamma\gamma$ final states in pp collisions at $\sqrt{s} = 8$ TeV

$$\sigma_{\text{tot}}^{\text{fid.}} = 16.8 \pm 0.1\ (\text{stat})\ \pm 0.7\ (\text{syst})\ \pm 0.3\ (\text{lumi})\ \text{pb} = 16.8 \pm 0.8\ \text{pb}$$

- Systematic uncertainties **decreased by up to a factor 2** w.r.t. the previous ATLAS measurement (7 TeV).
- **Precise probe of QCD infrared emissions** (a_{T}, ϕ_{η}^{*}), complementary to Drell-Yan.
  - **$\gamma\gamma$ originates from both $q\bar{q}$ and gg initial states.**
  - Important prerequisite for models aiming to describe the low q_{T} region in more complicated processes (e.g. coloured final states).
- **Fundamental test of pQCD** for both α_s and logarithmic series expansion.
  - Theory predictions get closer to data from NLO to NNLO but still more than 2σ away (2γNNLO, -16%)
  - Soft gluon resummation at NNLL (RESBOS) provides a good description of infrared emissions.

Summary

- ATLAS precision measurement of $\gamma\gamma$ final states in pp collisions at $\sqrt{s} = 8$ TeV

$$\sigma_{\text{tot}}^{\text{fid.}} = 16.8 \pm 0.1\ (\text{stat})\ \pm 0.7\ (\text{syst})\ \pm 0.3\ (\text{lumi})\ \text{pb} = 16.8 \pm 0.8\ \text{pb}$$

- Systematic uncertainties **decreased by up to a factor 2** w.r.t. the previous ATLAS measurement (7 TeV).
- **Precise probe of QCD infrared emissions** (a_{T}, ϕ_{η}^{*}), complementary to Drell-Yan.
  - **$\gamma\gamma$ originates from both $q\bar{q}$ and gg initial states.**
  - Important prerequisite for models aiming to describe the low q_{T} region in more complicated processes (e.g. coloured final states).
- **Fundamental test of pQCD** for both α_s and logarithmic series expansion.
  - Theory predictions get closer to data from NLO to NNLO but still more than 2σ away (2γNNLO, -16%)
  - Soft gluon resummation at NNLL (RESBOS) provides a good description of infrared emissions.
- Main background for $H \to \gamma\gamma$ and many searches for new physics at the LHC.
  - **SHERPA 2.2.1 (ME+PS at NLO) provides predictions at particle level in good agreement with the measurements.**

Measurements of integrated and differential cross sections for isolated photon pair production in 8 TeV pp collisions at ATLAS.

Thank you for your attention

Matthias Saimpert (DESY)

Rencontres de Moriond QCD

30/03/2017

Di-photon vertex identification

- Use of a neural-network algorithm to improve the reconstruction performance.
- Developed for the $H \to \gamma\gamma$ analysis

Phys. Rev. D. **90**, 112015 (2014)

validation with Z $\longrightarrow$ ee data (without considering electron tracks)

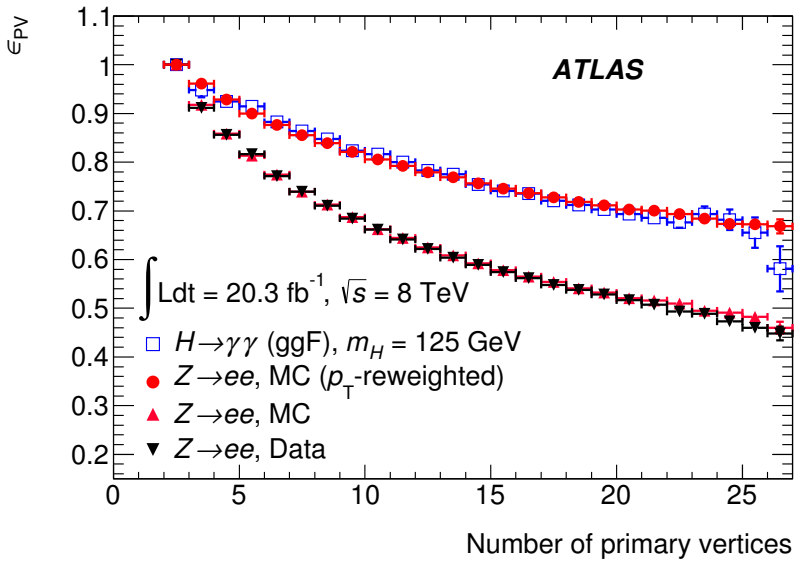

performance w.r.t. number of primary vertices

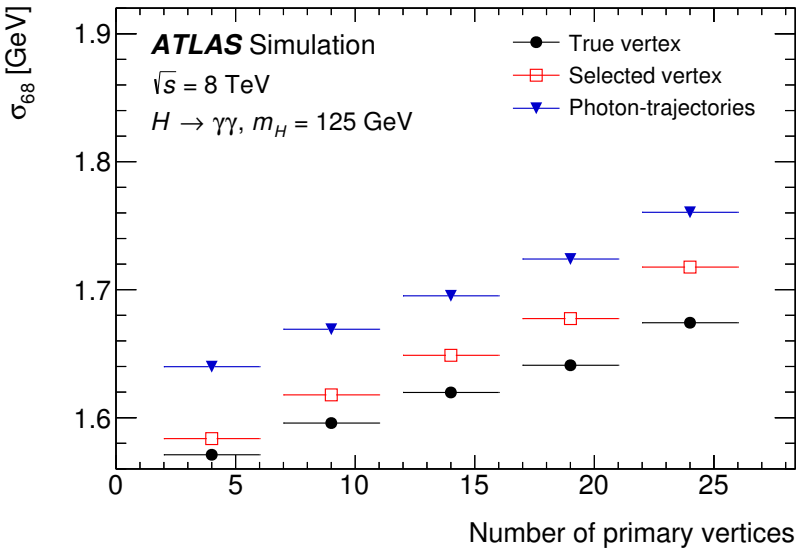

Isolation requirement optimization

Developed for the $H \to \gamma\gamma$ analysis

Phys. Rev. D. **90**, 112015 (2014)

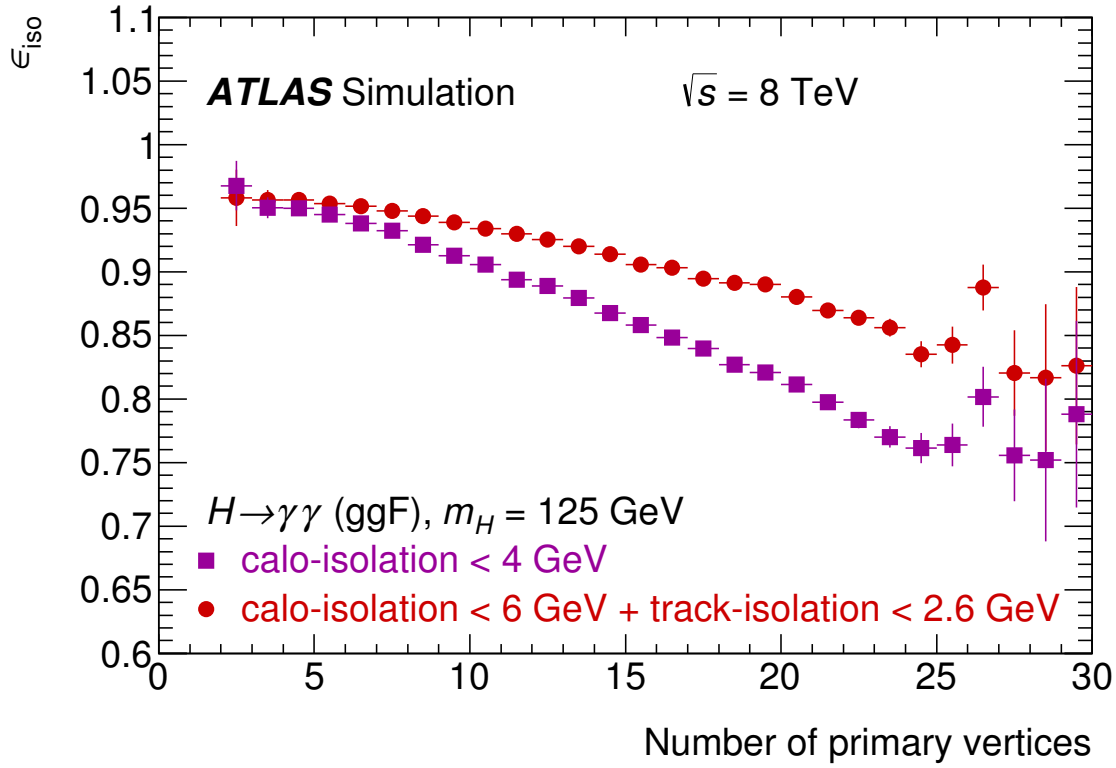

- flatter efficiency versus pileup
- flatter efficiency versus E_T^γ due to photon leakage corrections (not shown here)

Resolution of a_T and ϕ^*_η

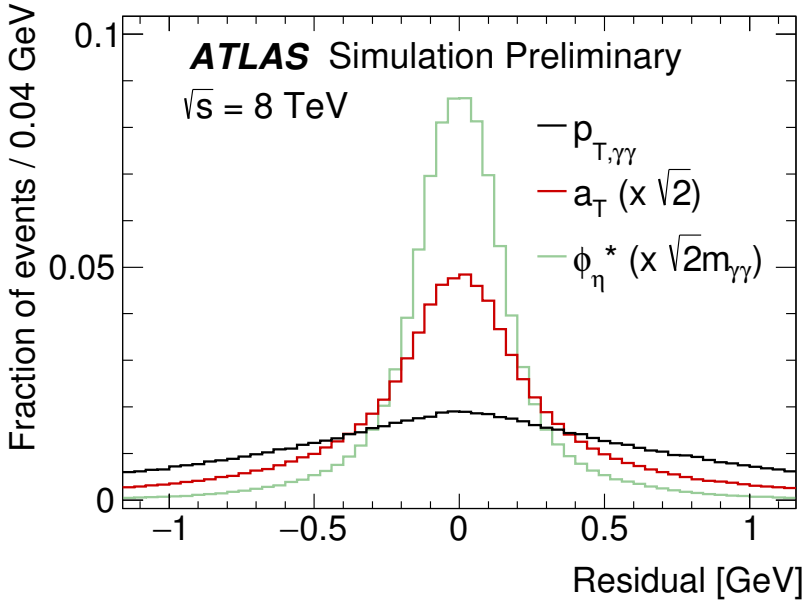

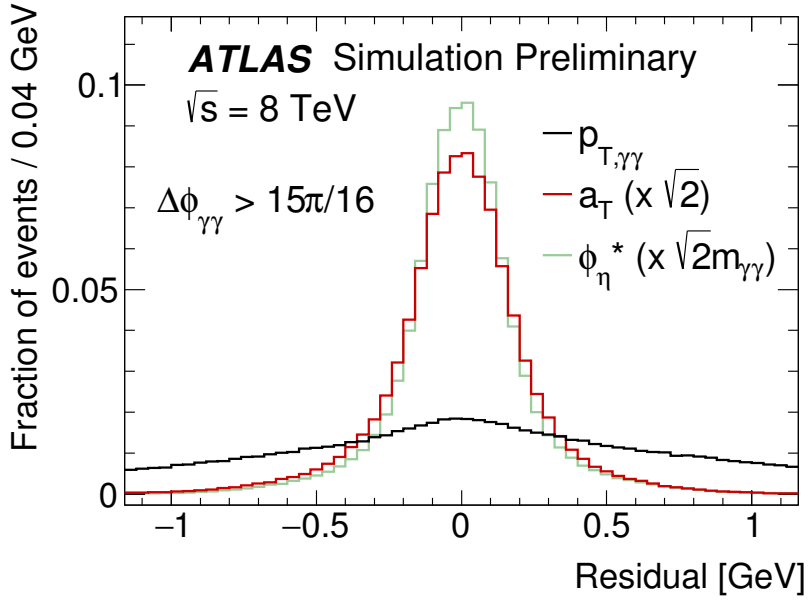

Calorimeter isolation variable explained

- $E_{\mathrm{T}}^{\mathrm{iso}}$: scalar sum of the $E_{\mathrm{T}} > 0$ GeV topo. clusters within a cone of size $\Delta R = 0.4$ around the photon candidate.
- contribution from pileup and underlying event subtracted on an event-by-event basis (jet area): provides estimate of average contribution in a wide η range.

  $\rightarrow$ downward fluctuations can lead to negative isolation energy values
- A fixed-size cluster is excluded to account for the photon energy. Leaking energy estimate provided by the simulation. Residual differences corrected using an inclusive photon data sample.

  $\rightarrow$ downward fluctuations can lead to negative isolation energy values
- Peak position driven by average corrections. Width driven by fluctuations around the average.

$E_{\mathrm{T},1}^{\mathrm{iso}}$ in the integrated signal region after fit

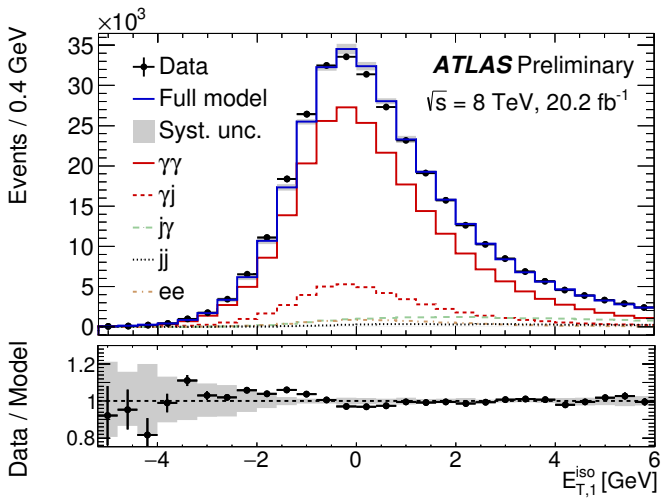

$E_{\mathrm{T},2}^{\mathrm{iso}}$ in the integrated signal region after fit

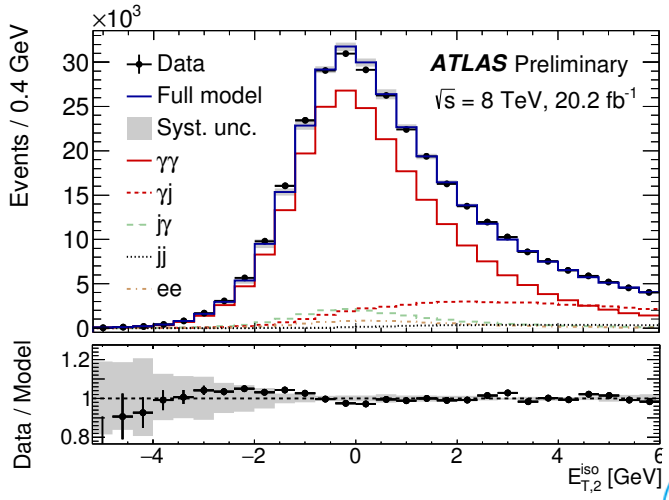

Sample composition

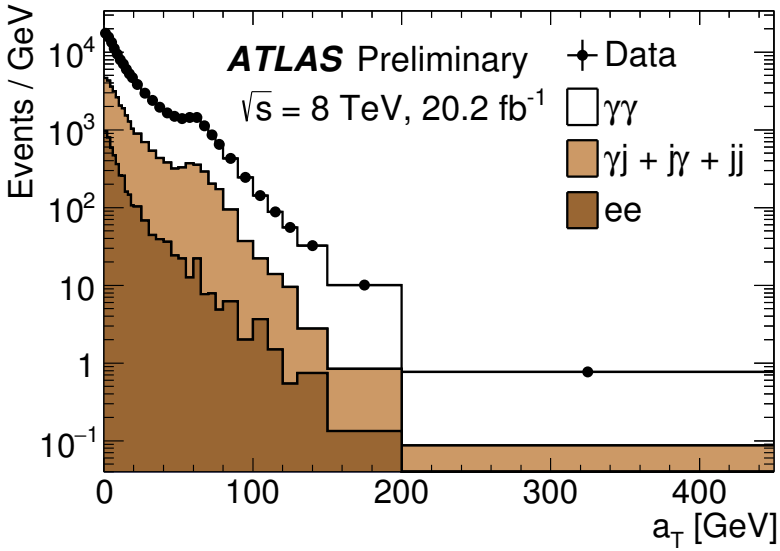

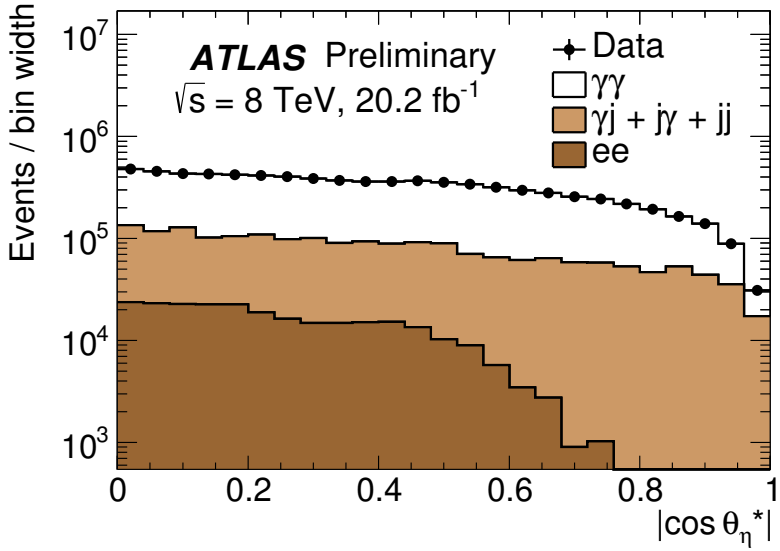

Sample composition

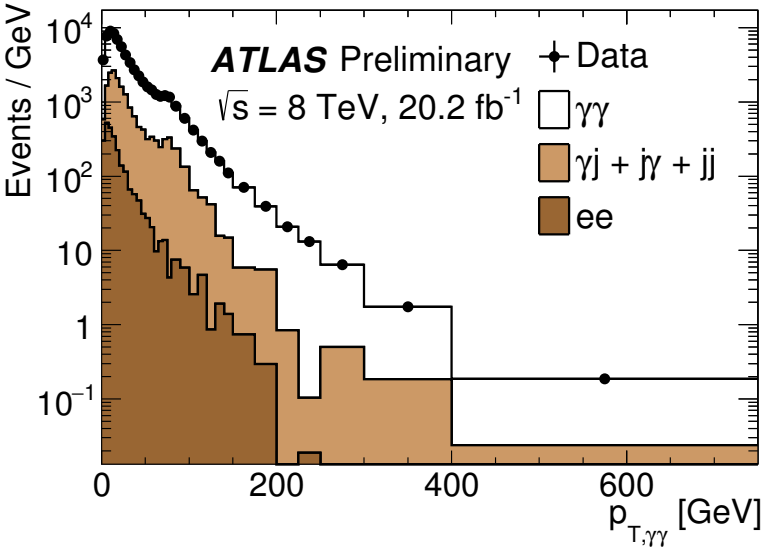

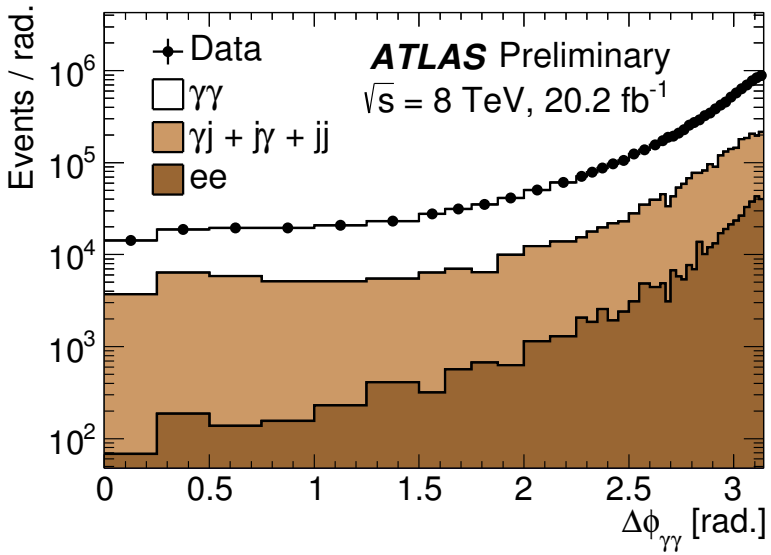

More on the Matrix method

- **Uses anti-isolated data ($\tilde{\mathbf{I}}$)** to derive identification efficiency for jets.

  $\rightarrow \beta_{\mathrm{data}} = \frac{n_{\mathrm{jet}}^{\mathbf{T}\tilde{\mathbf{I}}}}{n_{\mathrm{jet}}^{\tilde{\mathbf{T}}\tilde{\mathbf{I}}}}$, independent of isolation

- **Uses of γ MC** to derive identification efficiency for photons.

  $\rightarrow \alpha_{\mathrm{MC}} = \frac{n_{\gamma}^{\tilde{\mathbf{T}}\mathbf{I}}}{n_{\gamma}^{\mathbf{T}\mathbf{I}}}$, independent of isolation.

- **T$\rightarrow$TI** data-driven efficiency for photons (ϵ) and jets (f) [after some calculation]:

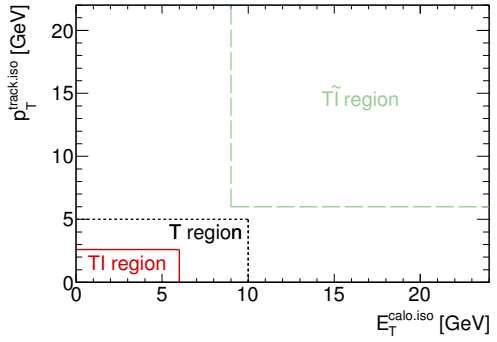

$$\epsilon = \frac{n_{\gamma}^{\mathbf{TI}}}{n_{\gamma}^{\mathbf{T}}} = \frac{n^{\mathbf{TI}} - \beta n^{\tilde{\mathbf{T}}\mathbf{I}}}{n^{\mathbf{T}} - \beta n^{\tilde{\mathbf{T}}}}; \qquad f = \frac{n_{j}^{\mathbf{TI}}}{n_{j}^{\mathbf{T}}} = \frac{n^{\tilde{\mathbf{T}}\mathbf{I}} - \alpha n^{\mathbf{TI}}}{n^{\tilde{\mathbf{T}}} - \alpha n^{\mathbf{T}}}$$

P = PASS isolation requirement (i.e. **TI**)
F = FAIL isolation requirement

$$\begin{pmatrix} N_{\mathrm{PP}}^{\mathrm{TT}} \\ N_{\mathrm{PF}}^{\mathrm{TT}} \\ N_{\mathrm{FP}}^{\mathrm{TT}} \\ N_{\mathrm{FF}}^{\mathrm{TT}} \end{pmatrix} = \mathbf{E} \begin{pmatrix} N_{\gamma\gamma}^{\mathbf{TT}} \\ N_{\gamma \mathrm{j}}^{\mathbf{TT}} \\ N_{\mathrm{j}\gamma}^{\mathbf{TT}} \\ N_{\mathrm{jj}}^{\mathbf{TT}} \end{pmatrix} \qquad \mathbf{E} = \begin{pmatrix} \epsilon_1\epsilon_2 & \epsilon_1 f_2 & f_1\epsilon_2 & \dots \\ \epsilon_1(1-\epsilon_2) & \epsilon_1(1-f_2) & f_1(1-\epsilon_2) & \dots \\ (1-\epsilon_1)\epsilon_2 & (1-\epsilon_1)f_2 & (1-f_1)\epsilon_2 & \dots \\ (1-\epsilon_1)(1-\epsilon_2) & (1-\epsilon_1)(1-f_2) & (1-f_1)(1-\epsilon_2) & \dots \end{pmatrix}$$

Photon identification efficiency at 8 TeV (unconverted)

Scale factors applied to simulation with associated uncertainty.

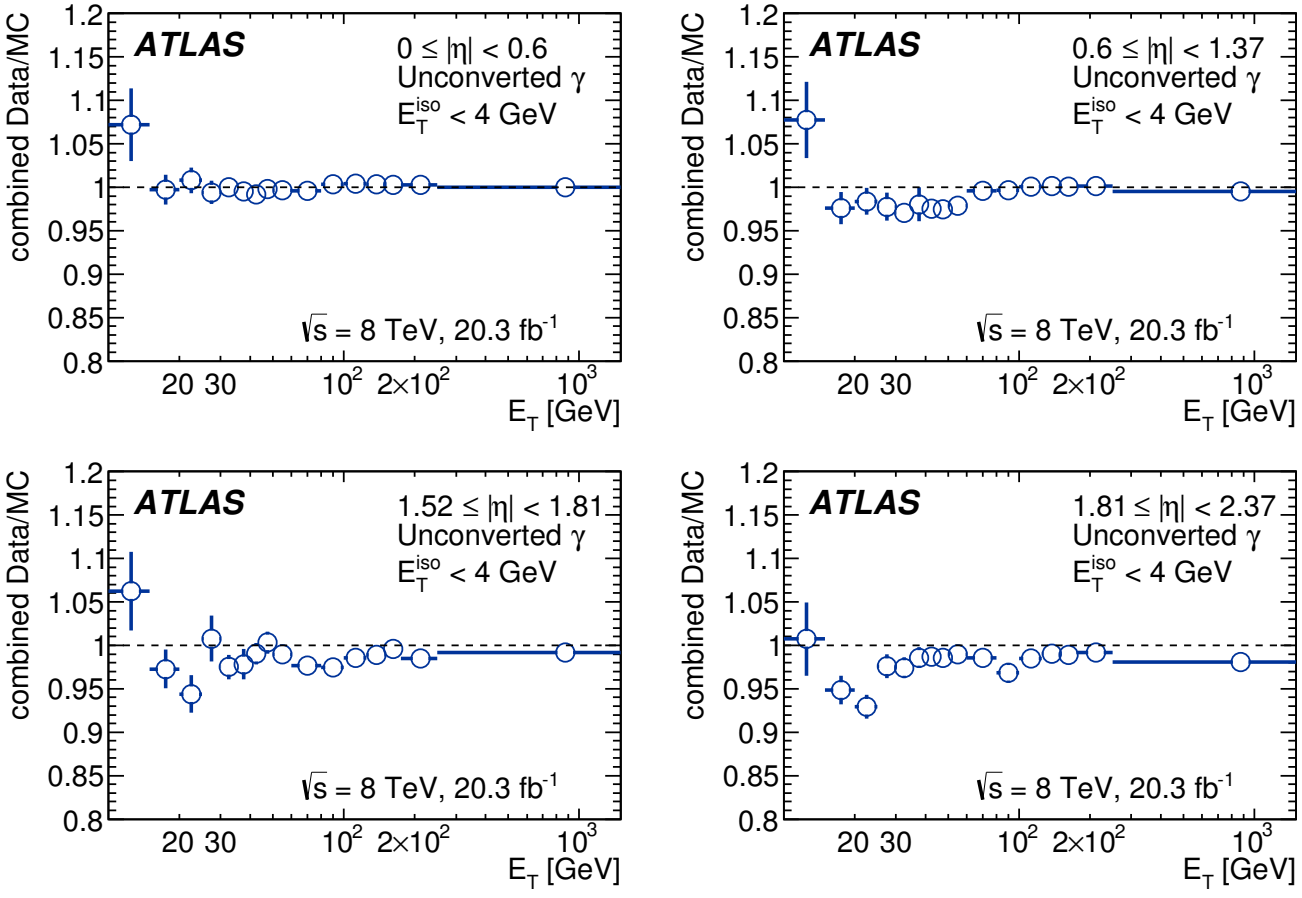

Eur. Phys. J. C **76** (2016) 666

Photon identification efficiency at 8 TeV (converted)

Scale factors applied to simulation with associated uncertainty.

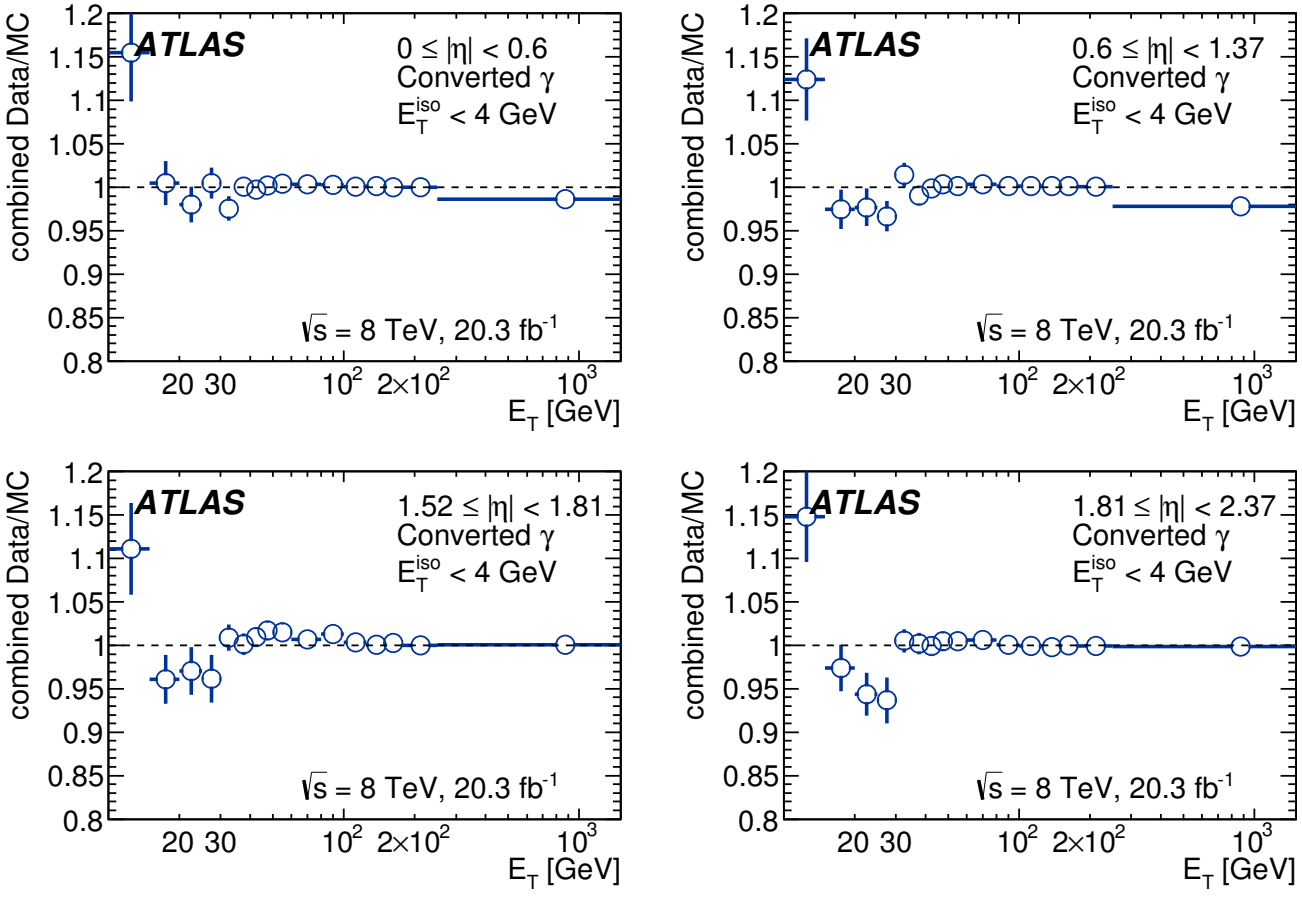

Eur. Phys. J. C **76** (2016) 666

Data/theory comparison for $m_{\gamma\gamma}$ and $p_{T,\gamma\gamma}$

$m_{\gamma\gamma}$ differential cross section measurement

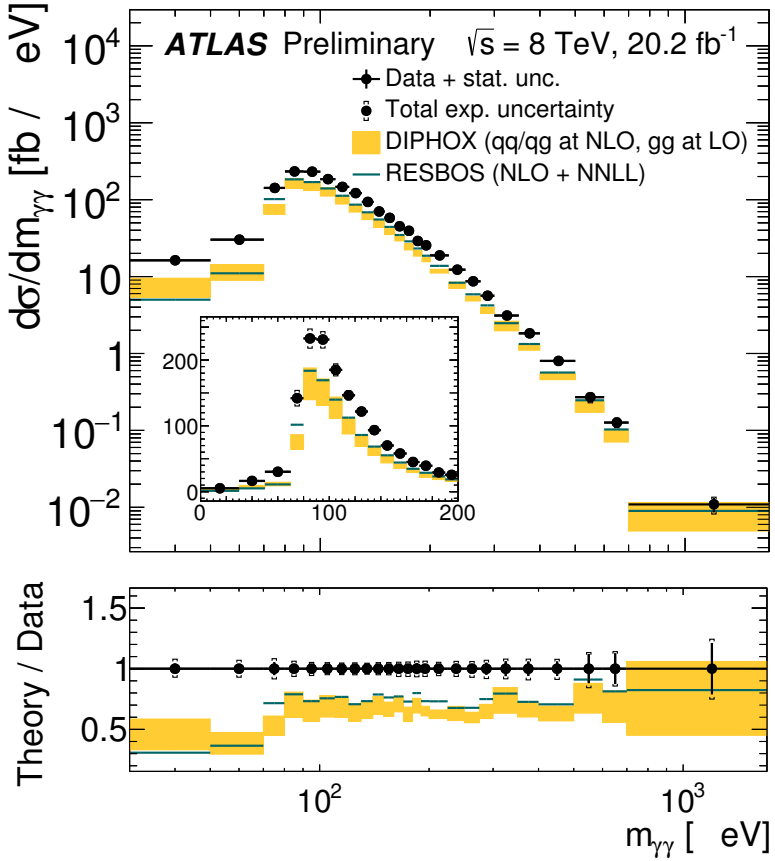

$p_{T,\gamma\gamma}$ differential cross section measurement

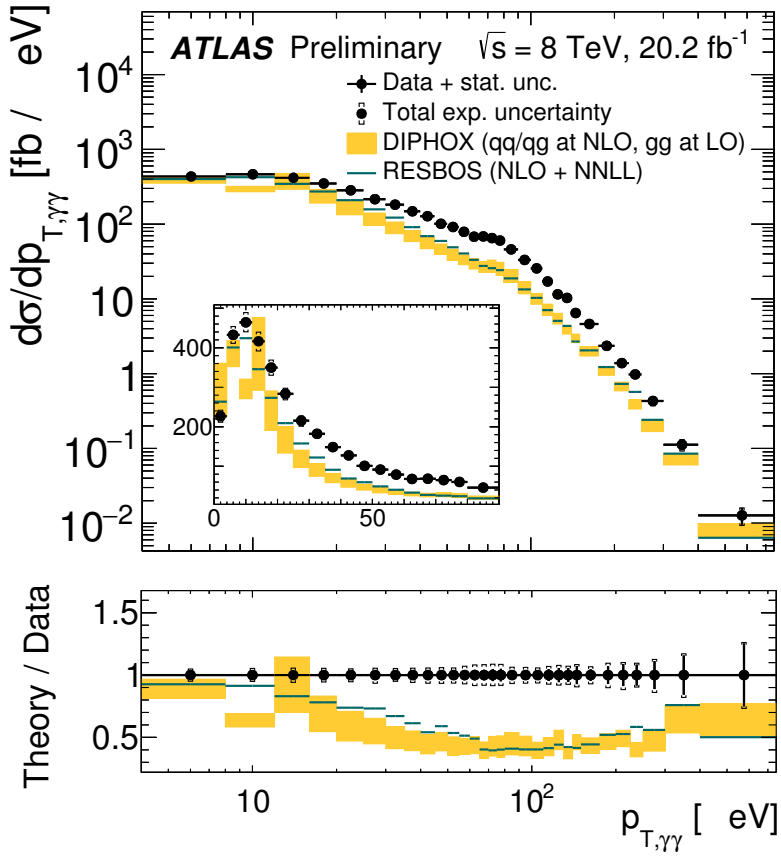

Data/theory comparison for a_T and ϕ^*_η

a_T differential cross section measurement

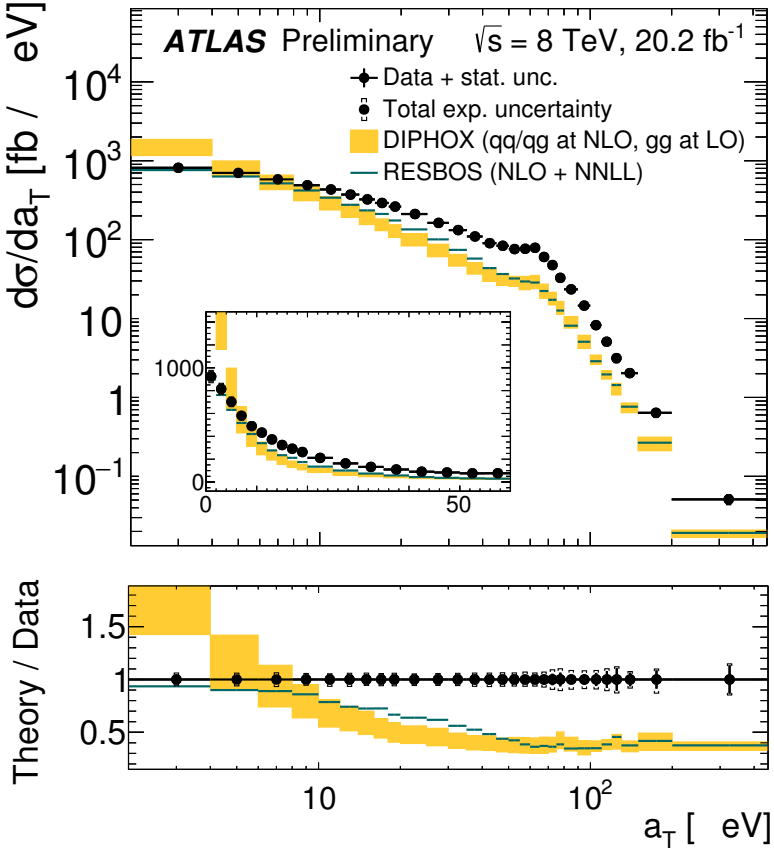

ϕ^*_η differential cross section measurement

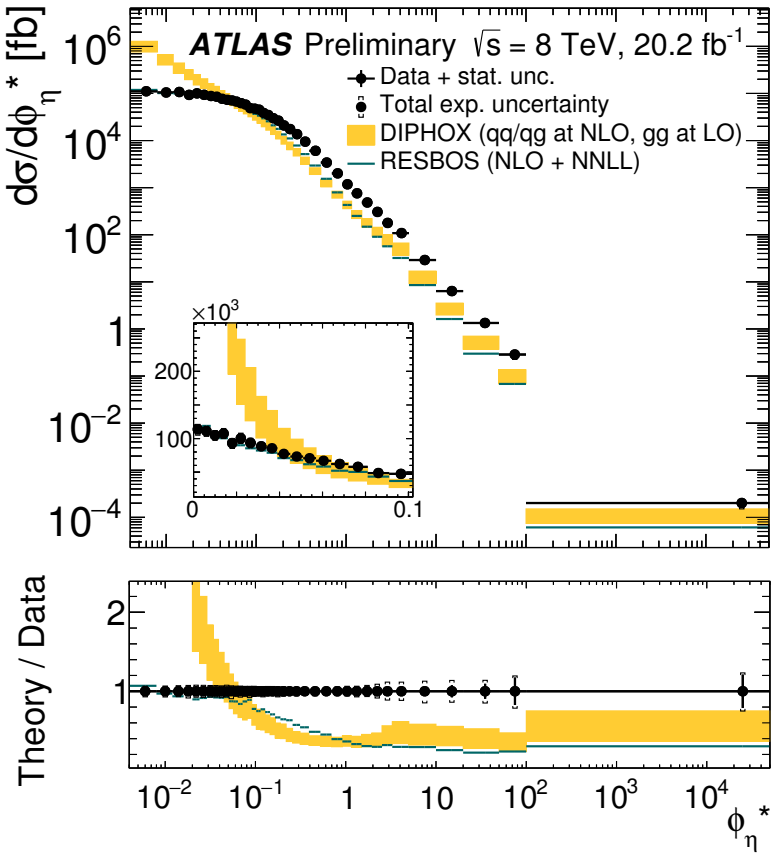

Data/theory comparison for $\Delta\phi_{\gamma\gamma}$ and $|\cos\theta^*_\eta|$

$\Delta\phi_{\gamma\gamma}$ differential cross section measurement

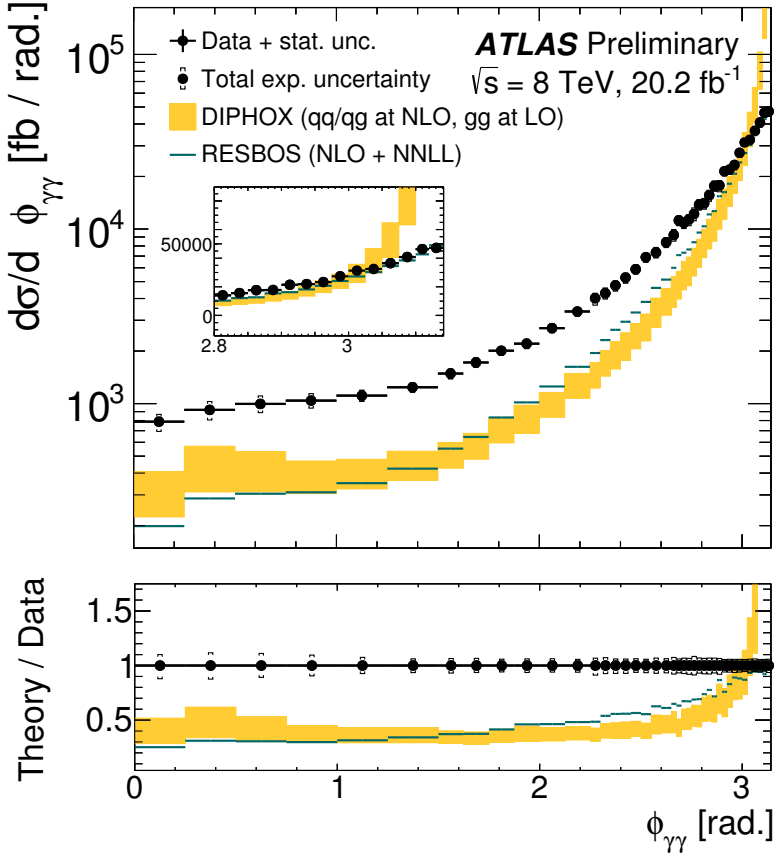

$|\cos\theta^*_\eta|$ differential cross section measurement

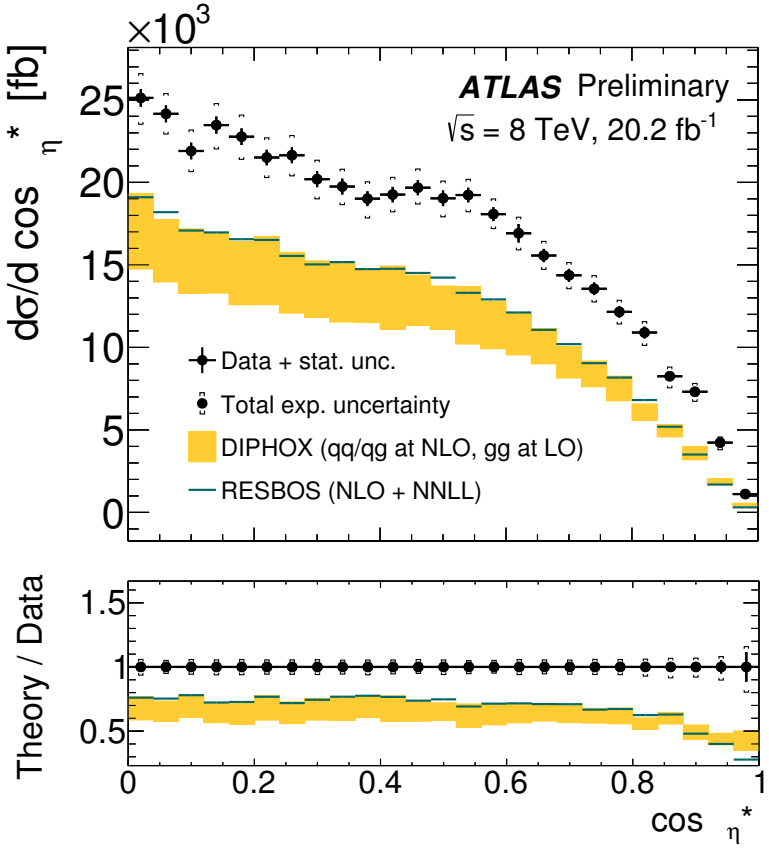

Data/theory comparison at 7 TeV (ATLAS)

JHEP **01** (2013) 086

$m_{\gamma\gamma}$ differential cross section measurement

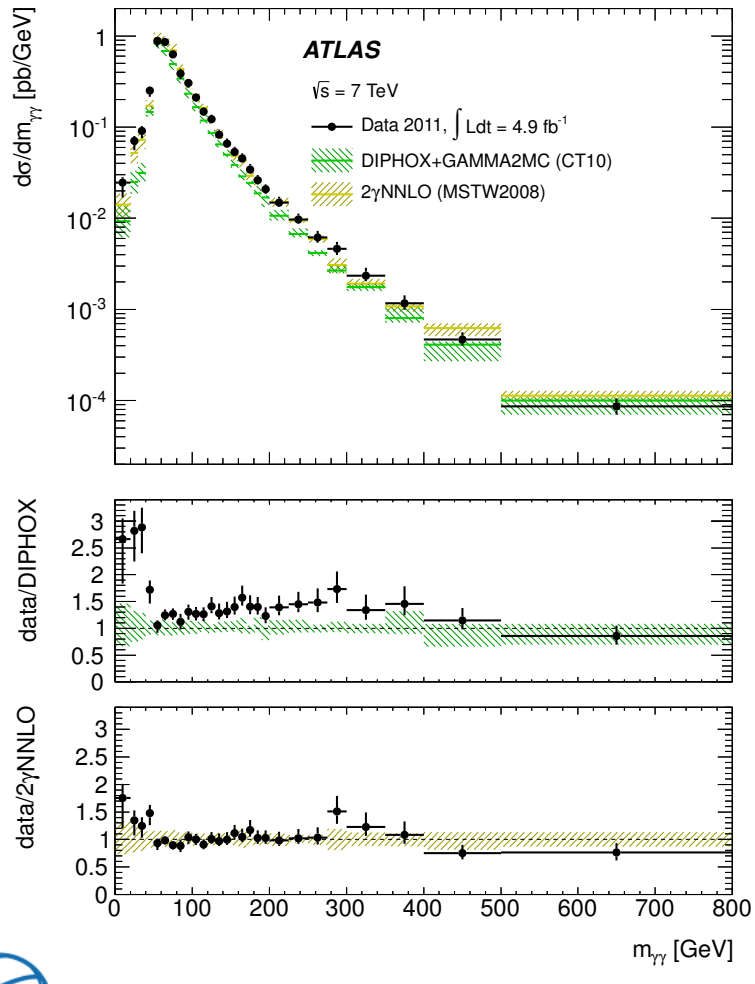

$\cos\theta^*_{\mathrm{CS}}$ differential cross section measurement

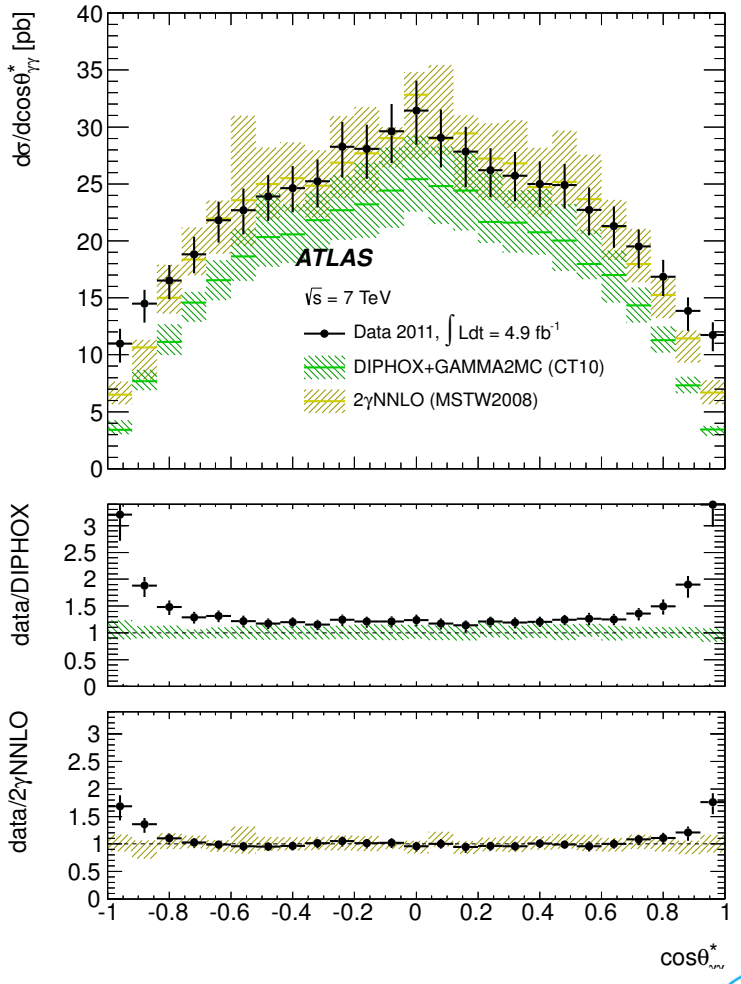

Data/theory comparison at 7 TeV (ATLAS)

JHEP **01** (2013) 086

$p_{T,\gamma\gamma}$ differential cross section measurement

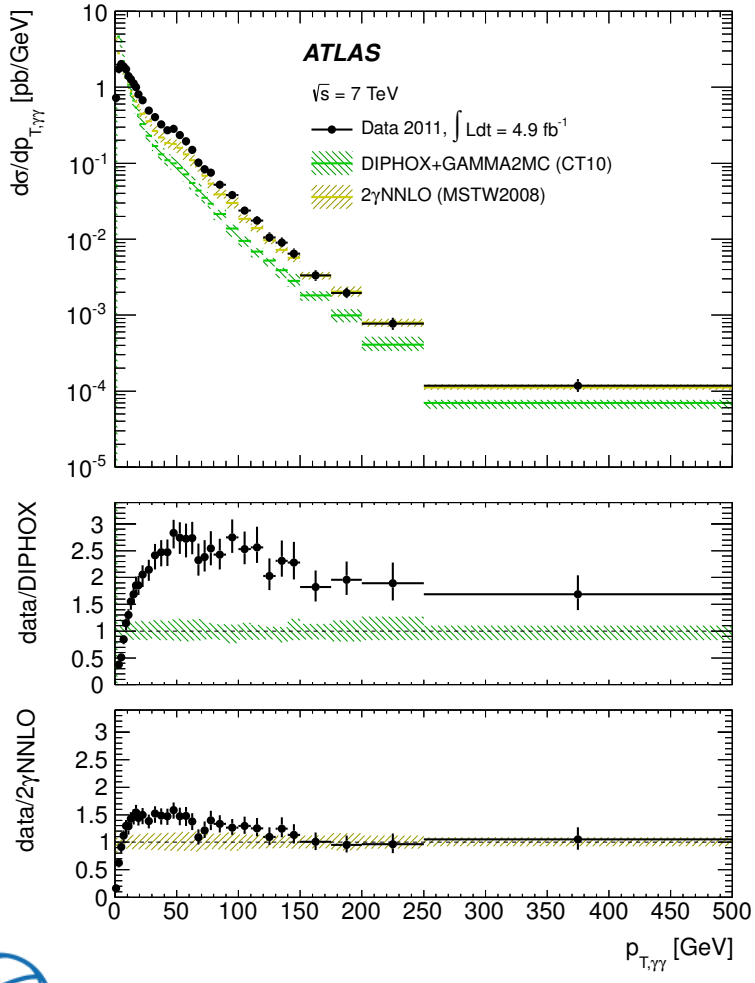

$\Delta\phi_{\gamma\gamma}$ differential cross section measurement

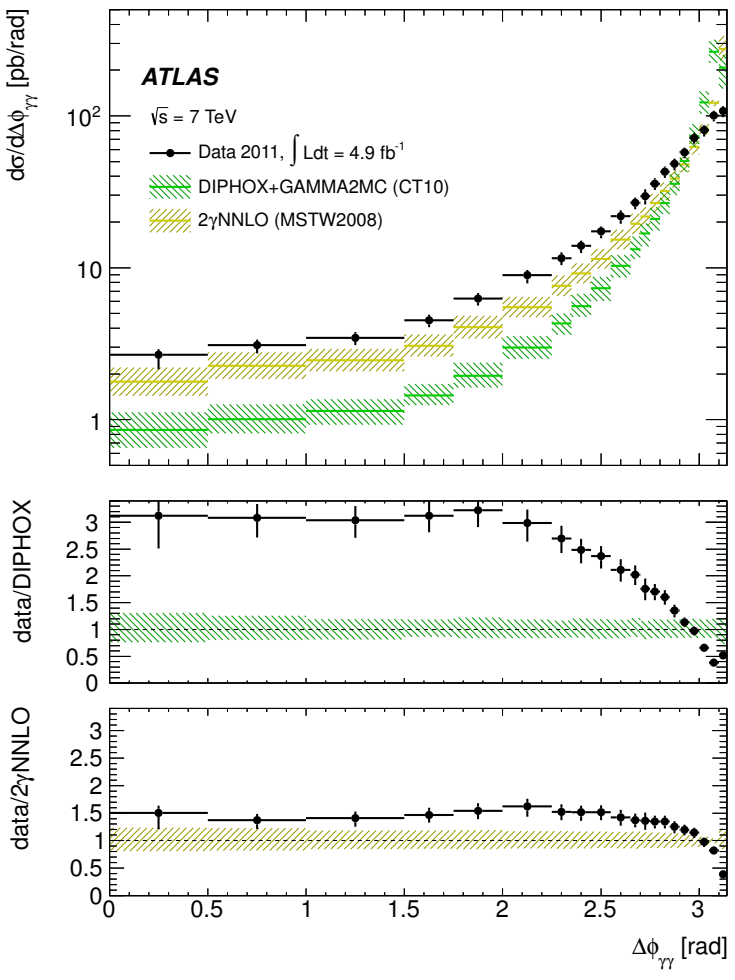

Data/theory comparison at 7 TeV (CMS)

Eur. Phys. J. C **74** (2014) 3129

$m_{\gamma\gamma}$ differential cross section measurement

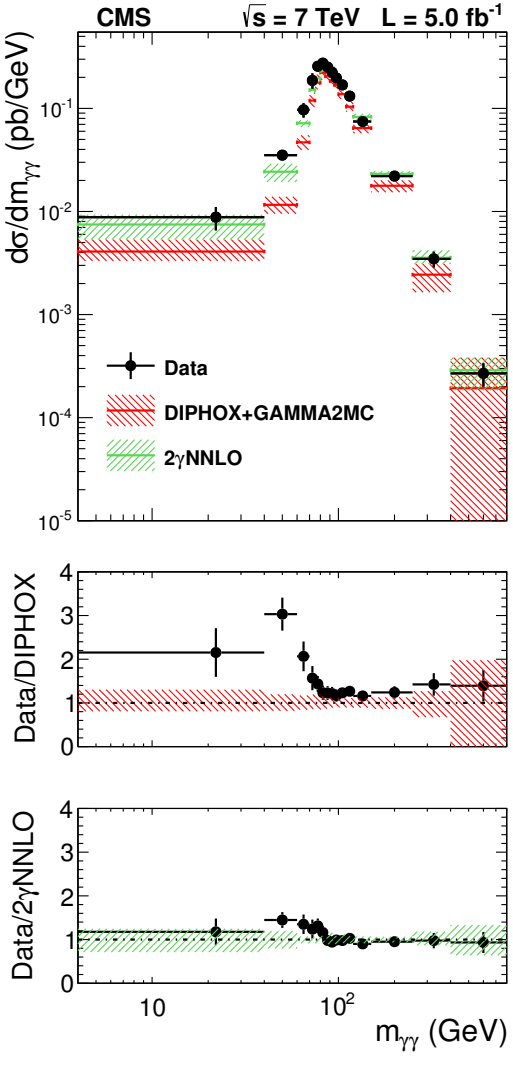

$\cos\theta^*_{\mathrm{CS}}$ differential cross section measurement

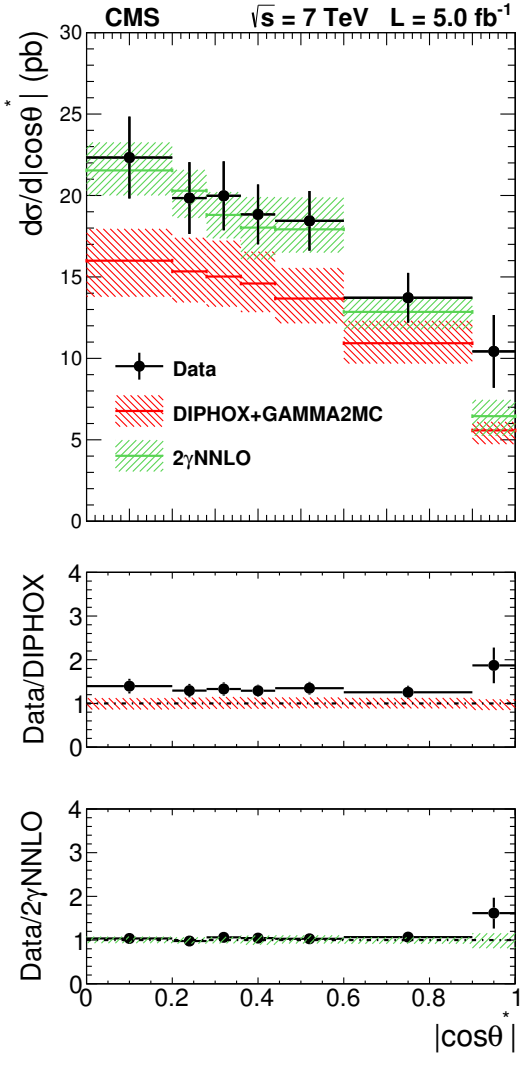

Data/theory comparison at 7 TeV (CMS)

Eur. Phys. J. C **74** (2014) 3129

$p_{T,\gamma\gamma}$ differential cross section measurement

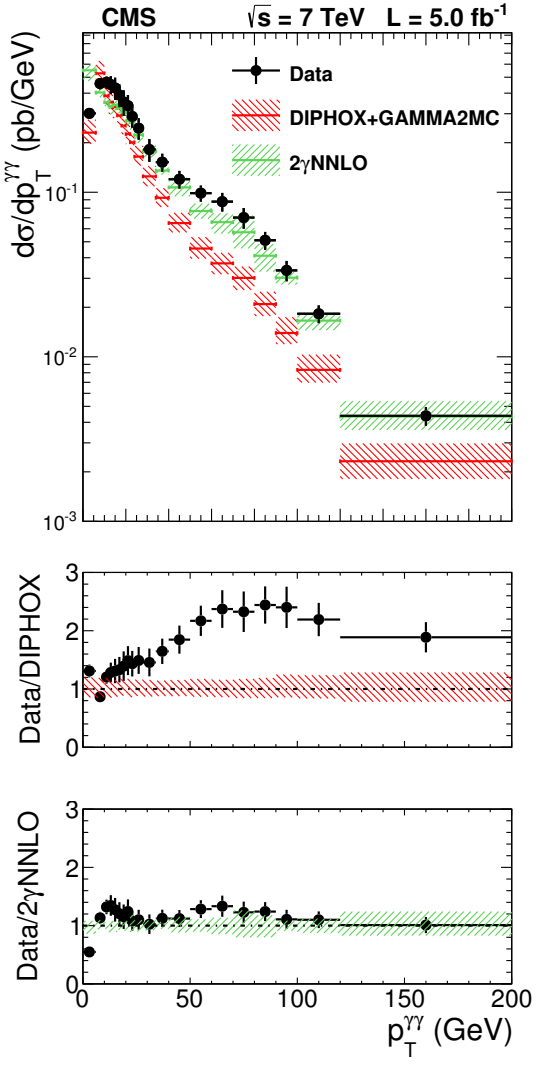

$\Delta\phi_{\gamma\gamma}$ differential cross section measurement